β1A integrin is a master regulator of invadosome organization and function.

Olivier Destaing, Emmanuelle Planus, Daniel Bouvard, Christiane Oddou, Cedric Badowski, Valentine Bossy, Aurelia Raducanu, Bertrand Fourcade, Corinne Albiges-Rizo, Marc Block

MBoC manuscrpt : E10-07-0580R in press

β1A integrin is a master regulator of invadosome organization and function

Olivier Destaing[1], Emmanuelle Planus[1], Daniel Bouvard[1], Christiane Oddou[1], Cedric Badowski[1], Valentine Bossy[1], Aurelia Raducanu[2], Bertrand Fourcade[1], Corinne Albiges-Rizo[1], and Marc R. Block[1]*

[1]Institut Albert Bonniot, Université Joseph Fourier; INSERM U823; CNRS ERL 3148, UJF site Santé, BP170, F38042 Grenoble cedex 09, France

[2] Department of Molecular Medicine, Max Planck Institut für Biochemie, Am Klopferspitz 18, D-82152 Martinsreid, Germany

* Correspondence to:

Marc R. Block, Institut Albert Bonniot, INSERM U823, équipe DySAD, Boite Postale 170, 38042 Grenoble cedex 09, France.

Tel: +33 476 54 95 51; Fax: +33 476 54 94 25; email: marc.block@ujf-grenoble.fr

Running title: β1 integrin control of invadosomes

Keywords: ECM degradation/integrins/invadopodia//PKC/podosomes

ABSTRACT

Invadosomes are adhesion structures involved in tissue invasion, characterized by an intense actin polymerization/depolymerization associated with β1 and β3 integrins and coupled to extracellular matrix degradation (ECM) activity. We induced the formation of invadosomes by expressing the constitutive active form of Src, SrcYF, in different cell types. Use of ECM surfaces micropatterned at the subcellular scale clearly showed that in mesenchymal cells, integrin signaling controls invadosome activity. Using $\beta1^{-/-}$ or $\beta3^{-/-}$ cells, it appeared that β1A but not β3 integrins are essential for initiation of invadosome formation. PKC activity was shown to regulate auto-assembly of invadosomes into a ring-like meta-structure (rosette), likely by phosphorylation of S785 on the β1A tail. Moreover, our study clearly showed that β1A links actin dynamics and ECM degradation in invadosomes. Finally, a new strategy based on fusion of the photosensitizer KillerRed to the β1A cytoplasmic domain allowed specific and immediate loss of function of β1A, resulting in disorganization and disassembly of invadosomes and formation of focal adhesions.

INTRODUCTION

Invadosome is a general term for structures implicated in tissue invasion processes that share similarities in organization, composition, dynamics, or function with podosomes, present in non-transformed cells (such as macrophages, osteoclasts, dendritic cells, endothelial cells, and smooth muscle cells), or invadopodia, present in cancer cells. This class of structure can be simply defined as an adhesion structure centered on an actin column, where intense actin activity takes place, and linked with localized extracellular matrix (ECM) degradation activity. Invadosomes can form isolated dot-like structures centered on a rapidly polymerizing actin column associated with actin regulators (such as cortactin, WASP, Rho GTPases, and fascin), adhesion molecules (such as paxillin, talin, and integrins), regulators of membrane dynamics (such as Tsk5, IQGAP, and VAMP7), metalloproteases, and regulatory kinases (such as FAK/Pyk2, PAK, and Src) (Linder and Aepfelbacher, 2003; Weaver, 2006; Ory *et al.*, 2008; Vignjevic and Montagnac, 2008; Albiges-Rizo *et al.*, 2009; Poincloux *et al.*, 2009). Moreover, like podosomes, invadosomes have the capacity to self-assemble into round meta-structures known as rosettes or rings, which can expand in diameter and fuse with each other. This treadmilling behavior is based on the coordinated assembly of new, individual actin columns, connected to each other by a "cloud" of F-actin at the outer rim, with disassembly of the original structure occurring at the inner rim of the rosette (Destaing *et al.*, 2003; Destaing *et al.*, 2005; Jurdic *et al.*, 2006; Badowski *et al.*, 2008).

Invadosomes were originally described in cells expressing the oncogene v-Src and have been reported in many subsequent studies (Marchisio *et al.*, 1984; Tarone *et al.*, 1985; Mueller *et al.*, 1992; Linder and Aepfelbacher, 2003; Bowden *et al.*, 2006). The essential role of the non-receptor tyrosine kinase c-Src in podosomes has been shown in $Src^{-/-}$ osteoclasts, where reduced bone resorption is associated with poorly functioning podosomes (Yoneda *et al.*, 1993; Hall *et al.*, 1994). The action of c-Src in podosomes is complex and essential for

initiation of podosome assembly, intensity of the actin flux, and architecture and disassembly of the structure (Luxenburg *et al.*, 2006; Ayala *et al.*, 2008; Destaing *et al.*, 2008). These adhesion structures can also be induced by activation of PKCs by Phorbol ester treatment, suggesting a synergistic activity of this pathway with the tyrosine kinase Src (Hai *et al.*, 2002; Tatin *et al.*, 2006).

Thus, it appears that both invadosome formation and self-assembly involve an inside-out signaling process. The question of which specific stimuli from the external environment (those participating in outside-in signaling) are able to induce invadosome formation remains unanswered. This led us to explore the functions of the integrin receptor families in the regulation of invadosome activity since these receptors integrate the composition, concentration, and compliance of the ECM. Integrins are heterodimers that oscillate between conformations having low and high affinity for the ECM. This switch corresponds to integrin activation and is favored by the disruption of the salt bridge between the α and β subunits induced by talin interaction with the β cytosolic domain of the integrin molecules (Shattil *et al.*, 2010). Moreover, this class of proteins has a strong link with ECM degradation, interacting directly with the membrane-associated metalloprotease MT1-MMP (also known as MMP14; (Galvez *et al.*, 2002). Although numerous studies have localized different integrins in podosomes and invadosomes, the specific functions of integrins in invadosomes have been poorly described. Indeed, αvβ3 is found in osteoclast podosomes and in invadosomes/invadopodia in many cancer cells (Zambonin-Zallone *et al.*, 1989): α3β1 in 804G carcinoma cells (Spinardi *et al.*, 2004); α4β1 in monocyte podosomes and β2 integrins in macrophage podosomes (Duong and Rodan, 2000); and β1 integrins in osteoclast podosomes (Helfrich *et al.*, 1996). Due to the role of podosomes in bone resorption by osteoclasts, a major role was assigned to αvβ3 integrin in this process based on the correlation between the strong increase in the expression of αvβ3 and the formation of podosomes during

osteoclast differentiation (Mimura *et al.*, 1994; Pfaff and Jurdic, 2001; Destaing *et al.*, 2003; Jurdic *et al.*, 2006). Moreover, perturbation of αvβ3 integrin by disintegrin modulates osteoclast migration and podosome formation (Nakamura *et al.*, 1999; Blair *et al.*, 2009). However, $\beta3^{-/-}$ mice show only a slight increase in bone mass in comparison to $Src^{-/-}$ osteoclasts, which are only associated with a disorganization of podosomes belts (McHugh *et al.*, 2000; Faccio *et al.*, 2003). In macrophages, Rho B inactivation results in decreased surface expression of integrins β2 and β3, while β1 surface expression remains constant. However, modification of this integrin pattern does not affect podosome formation (Wheeler and Ridley, 2007). On the other hand, the importance of β1 in invadopodia was suggested by activation of these integrins by soluble antibody, which leads to an increase in ECM degradation (Nakahara *et al.*, 1998).

To clarify the role of integrins in invadosome formation, auto-assembly, and organization, we have induced them by the expression of a constitutively active Src mutant, SrcYF, in cells in which either the β1 or β3 gene has been deleted, and performed reverse genetic analysis by expression of exogenous wild-type or mutant human integrin chains. Surprisingly, invadosome initiation and auto-assembly into rings were found to be strictly dependent on ECM signaling though β1 and not β3 integrins despite the high concentration of β3 in these structures. Invadosome auto-assembly likely involves the phosphorylation of Ser785 on the β1A cytosolic tail by PKC activity since PKC stimulation can be mimicked by the phosphomimetic mutants S785D or S785E. In addition, the modulation of β1A affinity by expression of β1A mutant in a genetic null background uncouples actin dynamics and the ECM-degradative activity of invadosomes. Finally, a new method to induce quick loss of function of β1A by photo-inactivation revealed that this integrin also plays a key role in invadosome metastructure stabilization. Thus, it appears that β1A is a key modulator of invadosome function in invasion processes.

MATERIALS AND METHODS

Antibodies and reagents

Antibodies for immunoblotting and immunofluorescence were obtained from the following commercial sources: rabbit anti-PhosphoTyr 418 Src and anti-phosphoTyr397 FAK (Invitrogen, Carlsbad, CA), mouse anti-Src (GD11, Millipore, Billerica, MA), mouse anti-actin (Sigma Aldrich, St. Louis, MO), mouse anti-paxillin (BD, Franklin Lakes, NJ), mouse anti-human β1 integrin (clone 4B7R, Beckton Dickinson, le Pont de Claix, France), and rat anti-mouse β1 integrin (MB1.2, Millipore, Fremont, CA), and rat anti-mouse β3 integrin (clone LucA5, Emfret Analytics, Würzburg, Germany).

Alexa 546-phalloidin, as well as Alexa 488, gelatin-Oregon green, and Alexa 488-, 546-, and 633-conjugated secondary antibodies were from Invitrogen.

Plasmids

pEGFP-actin vector was from Clontech (Palo Alto, CA). pBabe GFP-paxillin was provided by Dr. M. Hiraishi (Department of Molecular Biology, Osaka Bioscience Institute, Suita, Osaka, Japan), pBabe RFP-cortactin was engineered from the initial constructs, pDsRed-N1-cortactin from Dr P. Jurdic (ENS Lyon, France) and pcDNA3-mRFP (Addgen, Cambridge, MA).

Plasmids pFB-Neo-human β1-GFP, VASP-RFP, and pBabe-Src Y527F were the generous gifts of Dr Humphries (University of Manchester, Manchester, UK), Prof. Gertler (The David H. Koch Institute for Integrative Cancer Research, Massachusetts Institute of Technology, Cambridge, MA), and Dr K. Gil-Henn (Yale University, New Haven, CT), respectively.

For the pTRFP™ or KillerRed™-tagged human β1 construct, the pTRFP or KillerRed coding sequences were PCR-amplified from the original pTagRFP-N or pKillerRed-N vectors (Evrogen, Moscow, Russia) and used to replace GFP of pFB-Neo-human β1-GFP to generate an in-frame C-terminal fusion. pCLMGF-human β1 WT, pCLMGF-human β1 L747R, pCLMGF-human β1 D759A, pCLMGF-human β1 S785A, and pCLMGF-human β1 S785E constructs were made using the QuikChange XL site-directed mutagenesis kit (Stratagene, La Jolla, CA, USA) using the following primer pairs:

D759A: forward, 5'-gcttttaatgataattcatGCCagaagggagtttgc-3'; reverse, 5'gcaaactcccttctGGCatgaattatcattaaaagc-3';

S785D: forward, 5'cgggtgaaaatcctatttataagGATgccgtaacaactgtgg-3'; reverse, 5'ccacagttgttacggcATCcttataaataggattttcacccg-3';

S785E: forward, 5'cgggtgaaaatcctatttataagGAGgccgtaacaactgtgg-3'; reverse, 5'ccacagttgttacggcCTCcttataaataggattttcacccg-3';

S785A: forward, 5'cgggtgaaaatcctatttataagGCTgccgtaacaactgtgg-3'; reverse, 5'ccacagttgttacggcAGCcttataaataggattttcacccg-3'

Cell culture and infection

MEF $\beta3^{+/+}$ and $\beta3^{-/-}$ cells were the generous gift of Dr. Richard Hynes (The David H. Koch Institute for Integrative Cancer Research, Massachusetts Institute of Technology, Cambridge, MA). Mouse embryonic fibroblasts (MEF) isolated from $\beta1^{loxP/loxP}$ mice between embryonic day 12 and postnatal day 1, as described recently (Ferguson *et al.*, 2009), were the generous gift of Prof. Reinhard Fässler (Max Planck Institute of Biochemistry, Martinsreid, Germany).

A population of primary, mouse osteoblast-enriched cells was isolated from newborn mouse calvaria using a mixture of 0.3 mg/ml collagenase type I (Sigma-Aldrich, St. Louis, MO) and 0.25% trypsin (Invitrogen), as described previously (Bellows *et al.*, 1986; Bouvard *et al.*, 2007). Cells were grown in α-MEM containing 10% fetal calf serum (FCS). Primary osteoblasts (passage 2) were immortalized by transduction with a retrovirus expressing the large SV40 T antigen (Fassler *et al.*, 1995), cloned, and tested for their ability to express alkaline phophatase upon differentiation (Mansukhani *et al.*, 2000), as previously described (Bouvard *et al.*, 2007). At least five clones from floxed mice were isolated. Rescue of β1A integrin expression in cells was performed via retroviral infection using the pCLMFG-β1 vectors, as previously described (Bouvard *et al.*, 2007; Millon-Fremillon *et al.*, 2008). Cells were grown in DMEM containing glutamine and supplemented with 10% FCS and 1% penicillin/streptomycin. Cre adenovirus was purchased from the University of Iowa Gene Transfer Vector Core (Iowa City, IA). Maximal β1 depletion was achieved within 4 d. Cells were generally used for experiments between 6 and 9 days after Cre recombinase delivery. In most experiments, cDNAs were delivered via retroviral transduction following packaging in Phoenix-Eco or Phoenix-Ampho cells (American Type Culture Collection, Manassas, VA). Supernatant containing viral particles from transduced cells was harvested, filtered, and, following addition of 8 μg/ml polybrene (Sigma-Aldrich), was used to infect fibroblasts. For rescue experiments, cells were infected with exogenous β1 constructs, before addition of the CRE recombinase, to remove endogenous integrin. Before use, the cells were either serum-starved for 14 h in order or treated for 1 h with 2 μM phorbol myristyl acetate (PMA) to have SrcYF activity as the main signaling pathway in the cells. Either treatment allowed the development of a number of invadosomes and rosettes.

Micropatterning and functionalization

Patterned protein glass cover slips were performed according to (Guillou *et al.*, 2008) with slight modifications. Glass cover slips (22 × 22 mm) were washed in a solution of sulfuric acid and hydrogen peroxide (7:3, vol:vol) for 30 min, dried, and then dipped for 1 h in a solution of octadecyltrimethoxysilane and aminopropyltrimethoxy silane (3:1, mol:mol) (Sigma-Aldrich) in toluene. Positive photoresist resin (Shipley, S1805, Rhom & Haas Electronic Materials, Villeurbane, France) was spin-coated and cured according to the manufacturer's protocol to form a uniform, UV-sensitive film 0.5-µm thick. The coated cover slips were then insolated with UV light using a Karl Süss aligner (MJB3, SUSS MicroTec, Saint-Jeoire, France) at 436 nm and 15 mJ/cm^2 through a chromium mask. The irradiated pattern was revealed with microposit developer concentrate in deionized water (1:1, vol:vol) (Shipley, MF CD-26, Rhom & Haas Electronic Materials). The patterned cover slips were incubated for 1 h at 37°C in a solution of gelatin-RITC and 10 µg/ml vitronectin in phosphate-buffered saline (PBS). Substrates were rinsed in PBS and then in absolute ethanol in an ultrasonic water bath to dissolve the photoresist resin. Finally, either antiadhesive triblock copolymer Pluronic F127™ (Sigma-Aldrich) at a concentration of 4% in water for 1 h 30 min at 37°C, or a solution of FN7–10-FITC (Fibronectin type III domains 7-10 conjugated to FITC) at 5-15 µg/ml in PBS was adsorbed to the complementary pattern revealed after resin dissolution by ethanol for 1 hour at 37°C. Following a last rinse in PBS, 155 cells/mm^2 were seeded and incubated overnight, prior to fixation and staining.

Degradation assays

Coverslips were coated with 1 mg/ml gelatin-Oregon green, fixed with 4% (wt/vol) paraformaldehyde/0.5% glutaraldehyde for 30 min at 4°C, washed with 30 mg/ml sodium borohydride in PBS, sterilized with 70% ethanol, and rinsed once with PBS. Cells were seeded on the coverslips in culture medium for 2 h before being imaged for 14 h with a Zeiss Axiovert 200M equipped with a MicroMax 5MHz, 10× (NA 0.25) LDplan objective.

Microscopy and photoinactivation

For immunofluorescence analysis, cells were fixed with 4% paraformaldehyde in PBS, pH 7.4, and imaged with a Zeiss Axiovert 200M equipped with CoolSNAP HQ2, 63× (NA 1.4) Plan Apochromat and 100X (NA 1.4) Plan Apochromat objectives and a filter set to specifically detect Alexa488/GFP or Alexa546/pTRFP/KillerRed. At least 700 podosome structures were analyzed for each condition; representative data from to 3-5 independent experiments is presented.

For live imaging, cells were seeded at subconfluent densities in serum-coated, 35-mm, glass-bottom, 1.5mm-_thick dishes (Mattek, Ashland, MA) and allowed to grow for 12 to 48 h prior to imaging. DMEM was replaced by a CO_2-independent medium (Invitrogen), placed on a heated 37°C stage (Carl Zeiss Microimaging, Inc., Thornwood, NY), and imaged with the same Zeiss Axiovert 200M microscope set-up as previously described. Total internal reflection fluorescence (TIRF) microscopy was carried out with the same set-up as previously described and equipped with the TIRF 1 slider (Carl Zeiss microimaging GmbH, Gottingen, Germany).

For photoinactivation experiments, a Zeiss Axiovert 200M microscope equipped with a 63× (NA 1.4) Plan Apochromat objective and triple-filter set 25HE (excitation, TBP 405 + 495 + 575 [HE]; beam splitter, TFT 435 + 510 + 600 [HE], and emission, TBP 460 + 530 + 625 [HE]) (Carl Zeiss microimaging GmbH) was used for illumination. Cells were imaged as for live imaging, followed by a pause to allow illumination of the whole field of observation for 40-50 s (average, 45 s) with a 100W HBO mercury lamp at 100% power.

For fluorescence recovery after photobleaching (FRAP) experiments, an LSM510 ConfoCor microscope equipped with a 40× (NA 1.2) Plan apochromat objective (Carl Zeiss Microimaging GmbH) was used. The fluorescence recovery after bleaching time (3.2 s) was observed primarily in actin spots that persisted throughout the entire recovery time.

Imaging Series 7.0 (Universal Imaging, Downington, PA) software was used to mount .avi movies from image stacks. Images extracted from stacks were processed with Adobe Photoshop CS2 (Adobe Systems, San Jose, CA) and Image J (http://rsb.info.nih.gov/ij/). Significance of the differences between standard deviations was analyzed in Microsoft Excel with a F-test.

RESULTS

The ECM controls the assembly of invadosomes

To determine the role of ECM signaling on invadosome activity, we plated MEF transformed with constitutively active SrcYF on a layer of ECM micropatterned at the subcellular scale. Cells were seeded on alternate stripes of adhesive (gelatin-RITC mixed with vitronectin, red areas) and non-adhesive areas (Pluronic F127™, black areas), 5 and 10 µm in width, respectively. The invadosome rosettes were present on the adhesive stripes 95% of the time and continued to expand along the axis of these stripes (Figure 1A). These rosette formations suggested that the initiation of invadosome assembly is promoted by ECM signaling. Since integrins are the major actors in matrix sensing, we wanted to precisely define the roles played by specific subclasses of this receptor family. Therefore, we plated MEF-SrcYF onto patterned surfaces composed of alternating 5-µm stripes of RITC-vitronectin, which preferentially binds β3 integrins, and unlabelled fibronectin, which preferentially binds β1 integrins. Rosettes were more abundant on vitronectin, although the cells spread on both adhesive surfaces. In contrast, individual podosomes were seen on both surfaces (Figure 1B). However, on glass coverslips homogenously coated with fibronectin or vitronectin, MEF-SrcYF generated similar individual invadosomes and rosettes (data not shown). This result was reproduced with double patterned coverslips with either laminin and vitronectin, or collagen and vitronectin (Supplementary Figure S1B, C). These data indicated that invadosomes have a preference for vitronectin coated areas, suggesting an essential role of β3 integrin in invadosome activity (Figure 1B). However, most of the time, rosettes were initiated at the boundary of fibronectin and vitronectin areas (Supplementary Figure S1A). This peculiar location suggested that, despite their location on vitronectin, some outside-in signaling from fibronectin, possibly through β1 integrins, was necessary to initiate invadosome self-organization.

To determine the importance of β1 and β3 integrins in invadosome activity we analyzed the locations of these molecules and compared them with those of β1 integrins after spreading of the cells on endogenous matrix (48-h culture on glass coverslips). Since F-actin was found to be a reliable marker of nascent and mature invadosomes (Badowski *et al.*, 2008), double staining with either β1 and paxillin, or β3 antibodies and phalloidin, was carried out. Confocal scanning microscopy showed colocalization of β3 and F-actin, while β1 integrins were mostly excluded from the rosettes and accumulated at the outer rim, suggesting a possible function in newly formed invadosomes (Figure 1C). The early assembled invadosomes contain mostly the actin core, including cortactin. Detection of the active conformation of β1A was carried out after external addition in the medium of 9FG7 antibody directly-conjugated to FITC and visualized by TIRF microscopy on living cells expressing cortactin-mRFP. This analysis revealed that β1 integrins did not colocalize with cortactin and, rather, were in close proximity to the rim of the invadosome rosette (Figure 1D). Although β1 integrins accumulate around rosettes, our results did not support a structural role for them, in contrast to β3 integrins, which mediate adhesion and are a component of the mature invadosome.

β1 integrins are key regulators of invadosome formation

To investigate the involvement of β3 integrins in invadosome assembly, we induced these structures in $\beta3^{+/+}$ and $\beta3^{-/-}$ MEF by expressing the constitutively active form of Src. Surprisingly, MEF-SrcYF $\beta3^{-/-}$ cells displayed invadosome rosettes, although these structures were narrower and exhibited less intense actin staining than those observed in MEF-SrcYF $\beta3^{+/+}$ cells (Figure 2A). In line with these findings, MEF-YFSrc established invadosomes rosettes on the β1 specific substrates laminin111 and collagen (not shown). Conversely, β1 depletion in MEF SrcYF $\beta1^{loxP/loxP}$ cells, generated by adenoviral delivery of Cre

recombinase, resulted in invadosome formation in less than 5% of cells (Figure 2B top panel, 2C). The invadosomes observed in this small percentage of cells were likely due to a lack of Cre expression in some uninfected cells, as shown by quantitative PCR (Figure 2D). β1 depletion in MEF-SrcYF $\beta1^{loxP/loxP}$ was characterized by an increase in cell spreading and reorganization of F-actin into more abundant stress fibers (Figure 2B, bottom panel).

To confirm this unexpected and dramatic effect of removal of β1 and generalize this finding to other cell types, we applied the same strategy of inducing invadosomes through SrcYF expression in selected pre-osteoblastic pOBL $\beta1^{loxP/loxP}$ cells purified after Cre treatment. As for MEFs, the expression of SrcYF induced the formation of individual invadosomes and rosettes in $\beta1^{+/+}$ preosteoblasts, but not in their $\beta1^{-/-}$ counterparts. This loss of β1 was also accompanied by an increase in stress fibers within the cell bodies (Figure 3A and D). These modifications suggested some impairment of Src activity. However, Western analysis of cell lysates did not reveal significant changes in either Y416 phosphorylation, which characterizes Src activation, or in total Src expression (Figure 3B). Thus, our data suggested that β1 integrins have an essential role in the initiation of invadosome assembly.

Activation of β1 integrins stimulates invadosome auto-assembly into rosettes

Most of the β1 integrins around the rosettes were stained with the 9EG7 monoclonal antibody, indicating that these receptors were bound to their ECM ligands and therefore likely in their high-affinity state (Figure 1D). To test the role of integrin activation in invadopodia dynamics, we carried out a structure-function study and re-expressed exogenous human β1 chains bearing the point mutation D759A, which is known to modulate β1 activation state, in $\beta1^{-/-}$ pOBL-SrcYF cells (Figure 3C). This mutation promotes the integrin high-affinity state by breaking the saline bridge to the nearby arginine residue on the α chain (Shattil *et al.*, 2010). This mutant showed a dramatic increase in rosette number compared to wild-type cells (Figure 3D). In conclusion, in addition to the involvement of β1A in the initiation of assembly

of individual podosomes, the activation of β1A integrins appears to potentiate invadosome auto-assembly.

PKC directly targets β1A integrin to control invadosome auto-assembly

Previous studies in the literature show that in addition to Src signaling, the activation of conventional PKCs promotes invadosome formation in a variety of cell types (Hai *et al.*, 2002; Tatin *et al.*, 2006). Indeed, under standard cell culture conditions, PMA treatment stimulated invadosome auto-assembly into rosettes in a manner similar to conditions of serum starvation (Figure 4A) Based on the treadmilling process in invadosome turnover (Badowski *et al.*, 2008), the increase in invadosome auto-assembly could be due to an increase in either rosette stability or dynamics. To address this question, live-cell imaging was carried out on pOBL-SrcYF cells stably expressing GFP-actin and grown in serum-supplemented DMEM in the presence or absence of PMA. In the absence of PMA the few rosettes that could be detected were quite stable over 30 min. Conversely, activation of PKCs largely decreased invadosome life-span to under 10 min, resulting in a dramatic increase in rosette expansion and turnover (Figure 4B). On the other hand, inhibition of PKCs by the general inhibitor BIM resulted in rapid dissociation of rosettes, while the formation of individual invadosomes was still observed (Figure 4B). In the cytosolic domain of the β1A integrin subunit, a number of serine and threonine residues have been shown to be potential PKC phosphorylation sites modulating integrin function (Stroeken *et al.*, 2000; Mulrooney *et al.*, 2001) (Figure 4C). Among those residues, S785 was previously shown to be strongly phosphorylated upon Src overexpression (Sakai *et al.*, 2001). To investigate the importance of the PKC-dependent signaling pathway on β1A in the invadosome auto-assembly process, we expressed the β1 integrin mutants S785A, or S785D or S785E (nonphosphorylable or phosphomimetic forms, respectively), in a null genetic background and modulated PKC activity with an activator (PMA) or inhibitor (BIM). Consistent with the view that S785 is a direct target of PKC, only

the phosphomimetic mutants S785D and S785E were able to stimulate invadosome auto-assembly into rosettes in the absence of PMA (Figure 4D). The same phosphomimetic mutants were partly resistant to BIM inhibition as compared to wild type and the nonphosphorylatable S785A mutant (Figure 4E). In addition, the S785A mutant poorly rescued rosette assembly following PMA treatment (supplementary Figure S2). Taken together, these data support the view that S785 on the β1 subunit is one of the primary targets of PKC in the regulatory pathway of invadosome rosette auto-assembly in cells.

β1 integrin downstream signaling links invadosome formation and ECM degradation properties

Since invadosomes are major sites of ECM degradation, we investigated the involvement of β1 integrins in this crucial invadosome function by quantifying gelatin-Oregon green surface degradation, normalized per cell, over time. Even in the absence of invadosomes, pOBL-SrcYF $\beta1^{-/-}$ cells showed very low, but significant, ECM degradation activity 4 h after plating on gelatin (Figure 5A, C). Quantification of the average fluorescence intensity of the digested area is an efficient way to determine the extent or the depth of digestion. It was clearly shown that surfaces degraded by pOBL-SrcYF $\beta1^{-/-}$ cells were poorly digested (Figure 5B) as compared with rescued cells. The same results were obtained for MEF-SrcYF cells (data not shown). As shown previously, this structure-function study allowed exploration of the function of β1A in the ECM degradative activity of invadosomes. Re-expression of wild-type human β1A integrin rescued the degradation phenotype of pOBL-SrcYF $\beta1^{-/-}$ cells in terms of extent and depth of the ECM digestion (Figure 5A, B). On the other hand, the rescue of pOBL-SrcYF $\beta1^{-/-}$ cells with human β1A D759A, a mutant that pre-activates the integrin, led to the formation of numerous invadosomes, but which poorly digested ECM. Since wild-type integrin cycles between low- and high-affinity states, this loss

of function when the high-affinity state is promoted suggests the importance of the cycle of β1 activation/inactivation in this process. Thus, modulation of the β1A integrin activation state allowed, for the first time, the uncoupling of invadosome formation and ECM degradation activity. Moreover, regulation of invadosomes by PKC through phosphorylation of Ser785 was shown to be an essential step in activating invadosome ECM degradation properties. Indeed, the nonphosphorylatable mutant S785A of β1A strongly reduced the average surface area digested per cell, without affecting the depth of the degradation (Figure 5B). Conversely, the phosphomimetic β1A mutant S785D dramatically increased invadosome ECM degradation activity. Thus, not only the affinity state of β1, but also signaling pathways downstream of β_{1A}S785 phosphorylation (likely by PKC) control the coupling of invadosome assembly and ECM degradation activity.

β1 integrins stabilizes both rosettes and individual invadosomes

Having established that β1A integrins are important in initiating formation of individual invadosomes in the auto-assembly of rosettes, and to invadosome degradative function, we wanted to determine next whether signaling from β1A integrins located at the rosette periphery was required to simply initiate or to maintain rosette structure and dynamics. To address this question, we developed an improved photo-inactivation strategy based on the use of the photosensitizer KillerRed™ to achieve inducible loss of the β1A integrin chain. Briefly, we fused KillerRed™ to β1A in place of GFP and expressed it in MEF-SrcYF $\beta1^{loxP/loxP}$ cells. The endogenous *β1* gene was deleted in almost 100% of the cells 7 d post-Cre expression, as monitored by qPCR analysis of mouse *β1* mRNA (data not shown). In this genetic null background, the β1-KillerRed™ was functional since it allowed the assembly of rosettes and was correctly localized at their periphery. GFP-actin dynamics were followed after 45-s irradiation with red light in the KillerRed™ excitation spectrum (585 nm-615 nm).

KillerRed™ locally produces reactive oxygen species (ROS), resulting in the rapid inactivation of the protein to which it is fused. Indeed, photo-inactivation of β1- KillerRed™ resulted in a 95% decrease in red fluorescence, which was not recovered over the time of the observation (a maximum of 40 min after irradiation). This loss of β1A function led to the massive disorganization of the rosettes in under 20 min (Figure 6A, D).

ROS production in the cells could potentially have multiple indirect effects. To clearly show the specificity of this strategy, we first confirmed that the 45-s excitation with red light that resulted in KillerRed™ inactivation had no effect on invadosome structure, organization, and dynamics in cells expressing KillerRed™ alone in the cytosol (data not shown). Thus, non-localized ROS production after KillerRed™ irradiation had no effect on invadosomes or focal adhesions. To evaluate the potential toxicity of the 45-s red light irradiation and adsorption, KillerRed™ was replaced in the β1A fusion protein by TagRFP™, another photostable fluorescent molecule with an excitation/emission spectra similar to that of KillerRed™ (Supplementary Movie 2). Indeed, 45-s red light excitation of β1A-TagRFP™ had no effect on invadosomes, which remained stable for more than 40 min post-irradiation (Figure 6B, D). Finally, the nonspecific effects of ROS production on proteins and membranes in the vicinity of β1 after KillerRed™ excitation were investigated by simultaneous expression of β1A-GFP and β1A-KillerRed™ in a $\beta1^{-/-}$ background, since the two proteins were likely located in close proximity to each other (Supplementary Movie 3). In this environment, photo-inactivation of β1-KillerRed™ had no effect on β1A-GFP, which still allowed the formation of characteristic invadosome rings, as seen in non treated invadosome visualized by β1A-GFP and cortactin-TagRFP™ (bottom panel Figure 6C, Supplementary movie 8). These data clearly show that ROS produced by photoinactivation of KillerRed™ act only on the KillerRed™-tagged protein and not on surrounding macromolecules (Figure 6C, D).

This photo-inactivation strategy allowed us to monitor the specific effects of loss of β1A on pre-existing rosettes on a time scale of minutes. It is noteworthy that despite its specific localization around invadosome rings and its role in their initiation, inducible β1A depletion did not lead to progressive dissociation of the actin cytoskeleton from the inside to the outside of the rosettes, as would be expected because new actin structures are formed at the outer rim of the ring while older parts of the structure are disassembled at its inner rim) (Figure 6A). Soon after photo-inactivation, the polymerization of GFP-actin was not blocked, but rather formed unstable waves inside the rosette before the disorganization of these structures (Supplementary Movies 1, 7). Instability in the actin-polymerization domains within the rosette was followed by the complete collapse of the structure and increased cell spreading associated with the rapid formation of stress fibers (Supplementary Movie 1). Occasionally, GFP-actin signals reminiscent of the localization of invadosomes remained (Figure 6A).

Photo-inactivation of β1A integrins reveals the integrin functions in invadosome organization

To understand the mechanism underlying the GFP-actin-polymerization defect seen after loss of β1A function, the dynamics of the activity of the actin regulator cortactin fused to GFP was monitored (Supplementary movie 4). β1 photo-inactivation was rapidly followed by the dissociation of cortactin from invadosomes, explaining the perturbation of actin dynamics (Figure 7A). Similarly, the dynamics of adhesion molecules such as paxillin and β3-GFP integrins were analyzed (Supplementary Movies 5 and 6). In particular, the induction of β1 loss of function led to paxillin disorganization in invadosomes, although a fraction of this GFP-tagged protein remained localized at the previous site in the rosette (Figure 7B). This was also the case for β3-GFP but with this specific marker, it was clearer that invadosome

disorganization was associated with massive new formation or growth of focal adhesions (Figure 7C, red arrows). This rapid reorganization of the cellular adhesive structures was consistent with our observations of the formation of multiple stress fibers in response to β1 photo-inactivation (Supplementary Movie 1). In conclusion, despite its peripheral localization in the rosette, β1A integrin is a master regulator of invadosome assembly, organization, and stability.

DISCUSSION

Based on their high content and variety of integrins, invadosomes are integrin dependent adhesive structures associated with intense actin dynamics and responsible for local ECM degradation. The role of a specific integrin type in invadosome regulation is unclear, due to trans-dominant activities among the integrin classes and the lack of specificity of the tools used such as specific inhibitors or antibodies. Herein, we used the power of genetic to understand the role of two major integrins classes (those pairing with β1A and β3 chains) in the formation and dynamics of invadosomes. This strategy is based on the induction of invadosomes by SrcYF expression in a β1 or β3 null genetic background. Thus we are coupling the historical experiment by Tarone *et al.*, 1985 with the re-expression of wild type or mutant β chains allowing a straightforward reverse genetic analysis of β1A or β3 integrins functions in invadosomes.

Although the rosette assembly associated with the colocalization of β3 and F-actin on patterned surfaces has clearly shown preferential invadosome localization on vitronectin, MEF SrcYF $\beta3^{-/-}$ cells form invadosome rosettes, indicating that other integrin types can compensate the loss of β3. This finding confirms previous data showing that $\beta3^{-/-}$ osteoclasts are able to form podosomes (Faccio *et al.*, 2003).

On the contrary, the specific role of the β1 chain in initiating invadosome assembly is highlighted by the fact that the loss of β1 resulted in the complete disappearance of both individual and self-assembled invadopodia in primary cells and cell lines. These data do not fit with an earlier study reporting the presence of invadosome rosettes in the β1null cell lines Gβ11 and GD25 transformed with SrcYF. In that case however, the re-expression of the β1A double mutant (Y783F, Y795F) that poorly respond to Src transformation (Sakai *et al.*, 2001) clearly showed a trans dominant negative effect on invadosome formation, pointing to a major role of this integrin chain in invadosome formation (Huveneers *et al.*, 2008). Since these studies were using immortalized cells lines from knockout embryonic cells, one may assume that other compensatory mechanisms may have been at work. Indeed, in our hands, isolated clones of pOBL SrcYF $\beta1^{-/-}$ cells which normally do not form invadosomes, can form few invadosome rosettes after numerous passages in culture, suggesting that these immortalized cells lines start to set up compensatory mechanisms that rescue the formation of these adhesion structures (data not shown). At a first glance, and despite its localization around the rosette, the importance of β1 integrin is surprising since this integrin class appeared in wild type cells to be excluded from invadosomes, which contain mostly β3 integrin chains. However, immunostaining revealed an increased concentration of β1 at the outer rim of the rosettes. Since no colocalization with cortactin, a marker of nascent and mature invadopodia and invadosomes (Artym *et al.*, 2006; Badowski *et al.*, 2008) was observed, it is likely that β1integrins do not belong to the F-actin architecture composing invadosomes, but rather form a signaling platform to initiate invadosome assembly. In order to test this hypothesis, we developed a new approach to inactivate integrins at the minute time scale. The specific photo-inactivation of β1- KillerRed™ showed that this integrin loss induced a rapid collapse of the whole structure, indicating that the β1 chain is required not only to initiate invadosome assembly, but also to control the stability of the structure during the entire life span of the

rosette. This β1 functional ablation allowed us also to observe the rosette collapse from the outside to the inside. Thus, it appears that β1A integrins can signal at distance to control the disassembly processes occurring at the inner rim of invadosomes (Badowski *et al.*, 2008). Moreover, some residual F-actin, not associated with GFP-cortactin, forms an imprint after F-actin disassembly following photo-inactivation corresponding to the initial rosette. This strongly suggests the presence of two distinct actin network in the rosette: the actin cores with high cortactin content that depend on β1 signaling, and a more stable actin cloud around individual podosomes that is reminiscent of the radial actin arrays observed in macrophage or in the sealing zone of osteoclasts (Evans *et al.*, 2003; Luxenburg *et al.*, 2007). Finally, photo-inactivation of β1A-KillerRed™ is followed by the formation of focal adhesions, providing another example of the well described competition between focal adhesions and invadosomes.

In order to explore the β1A dependent control mechanisms of invadosomes, we focus our attention on PKC which is in addition to Src, a major inducer of invadosomes or podosomes (Hai *et al.*, 2002; Tatin *et al.*, 2006). Indeed, under standard cell culture conditions, PKC activity induced by PMA treatment greatly stimulated invadosome and rosette formation. The precise role of PKC activity in invadosomes is unclear. PKCα and PKCδ were shown to allow β1 integrin activation (Brenner *et al.*, 2008). This latter finding could be indirect since another PKC, PKCθ was shown to regulate the integrin activator Rap1 (Letschka *et al.*, 2008). The other possibility is that PKC phosphorylate directly integrins. Indeed, serine 785 and threonine 788 and 789 on the cytoplasmic tail of this integrin are potential targets of PKC. Since it was previously shown that S785 phosphorylation alters cell spreading (Mulrooney *et al.*, 2001) and that this particular residue was over-phosphorylated upon Src over expression (Sakai *et al.*, 2001), phosphomimetic and the non-phosphorylable β1A mutants S785E and S785D or S785A,respectively, were expressed in $\beta1A^{-/-}$ SrcYF MEF and pre-osteoblasts cells. Phosphomimetic mutant expression strongly stimulated invadosome self-assembly in the

absence of PMA and the mutant became partially resistant to the general PKC inhibitor BIM. These results strongly suggest that the direct phosphorylation of β1A on serine785 by PKC is an important event in the regulation of in invadosome assembly. However, the partial inhibition of phosphomimetic β1A mutants by BIM treatment also suggests that in addition to the direct phosphorylation of the β1A chain, PKC stimulation by PMA acts at other different levels of invadosome assembly. This view is also confirmed by the fact that, BIM treatment does not fully mimic the collapse of the rosette after β1-KillerRed™ photo-inactivation, but rather leads to the dissociation of the rosette into individual invadosomes.

The characterization of the ECM degradation by the multiple cell lines that we generated allowed us to determine the involvement of β1 integrins in this process and in invasion. This integrin is essential for proteolytic function of invadosomes. We observed a dramatic decrease in ECM degradation in pOBL $\beta1^{-/-}$ SrcYF cells. This result was expected since despite the transformation of the cells by SrcYF, the loss of

the integrin chain was accompanied by an almost complete loss of invadosomes. More surprisingly, the level of ECM degradation did not correlate with the increase in rosette assembly. Indeed, the expression of the pre-activated β1A mutant D759A in a β1null genetic background resulted in a 2- to 3-fold increase in the rosette number, which was associated with a significant decrease in the ECM degradation. To our knowledge, this is the first report the uncoupling of invadosome formation and matrix degradation. This could be due to the property of β1A integrin to interact with the plasma membrane-associated metalloprotease MT1-MMP (also called MMP14), which localized to invadosomes and is essential for the ECM degradation (Galvez *et al.*, 2002; Steffen *et al.*, 2008). Interference with MT1-MMP trafficking at the plasma membrane revealed that MT1-MMP activation and cell invasiveness are tightly coupled (Uekita *et al.*, 2001; Steffen *et al.*, 2008). Several lines of evidence have now established that in addition to being endosomal passengers, an important function of

integrins is to direct the trafficking of other receptors and cargos (for review see (Caswell *et al.*, 2009)). One can hypothesize that the affinity state of β1A integrin could modulate MT1-MMP trafficking at the plasma membrane and therefore impair its activity at the cell surface. This hypothesis is supported by the fact that PKCα increase integrin trafficking (Ng *et al.*, 1999) and that expression of β1A S785D or S785E, which mimic PKC activation, results in increased ECM degradation.

In conclusion, our results support a central role of β1 integrin-dependent outside-in signaling pathways in the regulation of the multiple cell compartments involved in invadosome functions.

ACKNOWLEDGMENTS

We thank Mrs. Manaa Wafa for technical assistance and interest, Dr Richard Hynes and Dr R. Fässler for providing us with $\beta1^{-/-}$ MEFs and β1 knock out conditional mice, respectively, This work was supported in part by the NanoFab micro fabrication facility of Louis Neel Institute (CNRS UPR 5051), the Association pour la Recherche contre le Cancer, the Ligne Nationale Contre le Cancer (équipe labellisée), the Agence Nationale pour la Recherche program PIRIBIO, and the fond d'intervention du Pôle Chimie Sciences du Vivant of Université J. Fourier.

REFERENCES

Albiges-Rizo, C., Destaing, O., Fourcade, B., Planus, E., and Block, M.R. (2009). Actin machinery and mechanosensitivity in invadopodia, podosomes and focal adhesions. Journal of cell science *122*, 3037-3049.

Artym, V.V., Zhang, Y., Seillier-Moiseiwitsch, F., Yamada, K.M., and Mueller, S.C. (2006). Dynamic interactions of cortactin and membrane type 1 matrix metalloproteinase at

invadopodia: defining the stages of invadopodia formation and function. Cancer Res *66*, 3034-3043.
Ayala, I., Baldassarre, M., Giacchetti, G., Caldieri, G., Tete, S., Luini, A., and Buccione, R. (2008). Multiple regulatory inputs converge on cortactin to control invadopodia biogenesis and extracellular matrix degradation. Journal of cell science *121*, 369-378.
Badowski, C., Pawlak, G., Grichine, A., Chabadel, A., Oddou, C., Jurdic, P., Pfaff, M., Albiges-Rizo, C., and Block, M.R. (2008). Paxillin phosphorylation controls invadopodia/podosomes spatiotemporal organization. Molecular biology of the cell *19*, 633-645.
Bellows, C.G., Sodek, J., Yao, K.L., and Aubin, J.E. (1986). Phenotypic differences in subclones and long-term cultures of clonally derived rat bone cell lines. J Cell Biochem *31*, 153-169.
Blair, H.C., Yaroslavskiy, B.B., Robinson, L.J., Mapara, M.Y., Pangrazio, A., Guo, L., Chen, K., Vezzoni, P., Tolar, J., and Orchard, P.J. (2009). Osteopetrosis with micro-lacunar resorption because of defective integrin organization. Lab Invest *89*, 1007-1017.
Bouvard, D., Aszodi, A., Kostka, G., Block, M.R., Albiges-Rizo, C., and Fassler, R. (2007). Defective osteoblast function in ICAP-1-deficient mice. Development *134*, 2615-2625.
Bowden, E.T., Onikoyi, E., Slack, R., Myoui, A., Yoneda, T., Yamada, K.M., and Mueller, S.C. (2006). Co-localization of cortactin and phosphotyrosine identifies active invadopodia in human breast cancer cells. Experimental cell research *312*, 1240-1253.
Brenner, W., Greber, I., Gudejko-Thiel, J., Beitz, S., Schneider, E., Walenta, S., Peters, K., Unger, R., and Thuroff, J.W. (2008). Migration of renal carcinoma cells is dependent on protein kinase Cdelta via beta1 integrin and focal adhesion kinase. Int J Oncol *32*, 1125-1131.
Caswell, P.T., Vadrevu, S., and Norman, J.C. (2009). Integrins: masters and slaves of endocytic transport. Nat Rev Mol Cell Biol *10*, 843-853.
Destaing, O., Saltel, F., Geminard, J.C., Jurdic, P., and Bard, F. (2003). Podosomes display actin turnover and dynamic self-organization in osteoclasts expressing actin-green fluorescent protein. Molecular biology of the cell *14*, 407-416.
Destaing, O., Saltel, F., Gilquin, B., Chabadel, A., Khochbin, S., Ory, S., and Jurdic, P. (2005). A novel Rho-mDia2-HDAC6 pathway controls podosome patterning through microtubule acetylation in osteoclasts. Journal of cell science *118*, 2901-2911.
Destaing, O., Sanjay, A., Itzstein, C., Horne, W.C., Toomre, D., De Camilli, P., and Baron, R. (2008). The tyrosine kinase activity of c-Src regulates actin dynamics and organization of podosomes in osteoclasts. Molecular biology of the cell *19*, 394-404.
Duong, L.T., and Rodan, G.A. (2000). PYK2 is an adhesion kinase in macrophages, localized in podosomes and activated by beta(2)-integrin ligation. Cell Motil Cytoskeleton *47*, 174-188.
Evans, J.G., Correia, I., Krasavina, O., Watson, N., and Matsudaira, P. (2003). Macrophage podosomes assemble at the leading lamella by growth and fragmentation. The Journal of cell biology *161*, 697-705.
Faccio, R., Takeshita, S., Zallone, A., Ross, F.P., and Teitelbaum, S.L. (2003). c-Fms and the alphavbeta3 integrin collaborate during osteoclast differentiation. The Journal of clinical investigation *111*, 749-758.
Fassler, R., Pfaff, M., Murphy, J., Noegel, A.A., Johansson, S., Timpl, R., and Albrecht, R. (1995). Lack of beta 1 integrin gene in embryonic stem cells affects morphology, adhesion, and migration but not integration into the inner cell mass of blastocysts. J Cell Biol *128*, 979-988.
Ferguson, S.M., Raimondi, A., Paradise, S., Shen, H., Mesaki, K., Ferguson, A., Destaing, O., Ko, G., Takasaki, J., Cremona, O., E, O.T., and De Camilli, P. (2009). Coordinated actions of actin and BAR proteins upstream of dynamin at endocytic clathrin-coated pits. Dev Cell *17*, 811-822.

Galvez, B.G., Matias-Roman, S., Yanez-Mo, M., Sanchez-Madrid, F., and Arroyo, A.G. (2002). ECM regulates MT1-MMP localization with beta1 or alphavbeta3 integrins at distinct cell compartments modulating its internalization and activity on human endothelial cells. The Journal of cell biology *159*, 509-521.
Guillou, H., Depraz-Depland, A., Planus, E., Vianay, B., Chaussy, J., Grichine, A., Albiges-Rizo, C., and Block, M.R. (2008). Lamellipodia nucleation by filopodia depends on integrin occupancy and downstream Rac1 signaling. Experimental cell research *314*, 478-488.
Hai, C.M., Hahne, P., Harrington, E.O., and Gimona, M. (2002). Conventional protein kinase C mediates phorbol-dibutyrate-induced cytoskeletal remodeling in a7r5 smooth muscle cells. Experimental cell research *280*, 64-74.
Hall, T.J., Schaeublin, M., and Missbach, M. (1994). Evidence that c-src is involved in the process of osteoclastic bone resorption. Biochem Biophys Res Commun *199*, 1237-1244.
Helfrich, M.H., Nesbitt, S.A., Lakkakorpi, P.T., Barnes, M.J., Bodary, S.C., Shankar, G., Mason, W.T., Mendrick, D.L., Vaananen, H.K., and Horton, M.A. (1996). Beta 1 integrins and osteoclast function: involvement in collagen recognition and bone resorption. Bone *19*, 317-328.
Huveneers, S., Arslan, S., van de Water, B., Sonnenberg, A., and Danen, E.H. (2008). Integrins uncouple Src-induced morphological and oncogenic transformation. The Journal of biological chemistry *283*, 13243-13251.
Jurdic, P., Saltel, F., Chabadel, A., and Destaing, O. (2006). Podosome and sealing zone: specificity of the osteoclast model. European journal of cell biology *85*, 195-202.
Letschka, T., Kollmann, V., Pfeifhofer-Obermair, C., Lutz-Nicoladoni, C., Obermair, G.J., Fresser, F., Leitges, M., Hermann-Kleiter, N., Kaminski, S., and Baier, G. (2008). PKC-theta selectively controls the adhesion-stimulating molecule Rap1. Blood *112*, 4617-4627.
Linder, S., and Aepfelbacher, M. (2003). Podosomes: adhesion hot-spots of invasive cells. Trends in cell biology *13*, 376-385.
Luxenburg, C., Geblinger, D., Klein, E., Anderson, K., Hanein, D., Geiger, B., and Addadi, L. (2007). The architecture of the adhesive apparatus of cultured osteoclasts: from podosome formation to sealing zone assembly. PLoS One *2*, e179.
Luxenburg, C., Parsons, J.T., Addadi, L., and Geiger, B. (2006). Involvement of the Src-cortactin pathway in podosome formation and turnover during polarization of cultured osteoclasts. Journal of cell science *119*, 4878-4888.
Mansukhani, A., Bellosta, P., Sahni, M., and Basilico, C. (2000). Signaling by fibroblast growth factors (FGF) and fibroblast growth factor receptor 2 (FGFR2)-activating mutations blocks mineralization and induces apoptosis in osteoblasts. J Cell Biol *149*, 1297-1308.
Marchisio, P.C., Cirillo, D., Naldini, L., Primavera, M.V., Teti, A., and Zambonin-Zallone, A. (1984). Cell-substratum interaction of cultured avian osteoclasts is mediated by specific adhesion structures. The Journal of cell biology *99*, 1696-1705.
McHugh, K.P., Hodivala-Dilke, K., Zheng, M.H., Namba, N., Lam, J., Novack, D., Feng, X., Ross, F.P., Hynes, R.O., and Teitelbaum, S.L. (2000). Mice lacking beta3 integrins are osteosclerotic because of dysfunctional osteoclasts. The Journal of clinical investigation *105*, 433-440.
Millon-Fremillon, A., Bouvard, D., Grichine, A., Manet-Dupe, S., Block, M.R., and Albiges-Rizo, C. (2008). Cell adaptive response to extracellular matrix density is controlled by ICAP-1-dependent beta1-integrin affinity. J Cell Biol *180*, 427-441.
Mimura, H., Cao, X., Ross, F.P., Chiba, M., and Teitelbaum, S.L. (1994). 1,25-Dihydroxyvitamin D3 transcriptionally activates the beta 3-integrin subunit gene in avian osteoclast precursors. Endocrinology *134*, 1061-1066.

Mueller, S.C., Yeh, Y., and Chen, W.T. (1992). Tyrosine phosphorylation of membrane proteins mediates cellular invasion by transformed cells. The Journal of cell biology *119*, 1309-1325.
Mulrooney, J.P., Hong, T., and Grabel, L.B. (2001). Serine 785 phosphorylation of the beta1 cytoplasmic domain modulates beta1A-integrin-dependent functions. Journal of cell science *114*, 2525-2533.
Nakahara, H., Mueller, S.C., Nomizu, M., Yamada, Y., Yeh, Y., and Chen, W.T. (1998). Activation of beta1 integrin signaling stimulates tyrosine phosphorylation of p190RhoGAP and membrane-protrusive activities at invadopodia. The Journal of biological chemistry *273*, 9-12.
Nakamura, I., Pilkington, M.F., Lakkakorpi, P.T., Lipfert, L., Sims, S.M., Dixon, S.J., Rodan, G.A., and Duong, L.T. (1999). Role of alpha(v)beta(3) integrin in osteoclast migration and formation of the sealing zone. Journal of cell science *112 (Pt 22)*, 3985-3993.
Ng, T., Shima, D., Squire, A., Bastiaens, P.I., Gschmeissner, S., Humphries, M.J., and Parker, P.J. (1999). PKCalpha regulates beta1 integrin-dependent cell motility through association and control of integrin traffic. EMBO J *18*, 3909-3923.
Ory, S., Brazier, H., Pawlak, G., and Blangy, A. (2008). Rho GTPases in osteoclasts: orchestrators of podosome arrangement. European journal of cell biology *87*, 469-477.
Pfaff, M., and Jurdic, P. (2001). Podosomes in osteoclast-like cells: structural analysis and cooperative roles of paxillin, proline-rich tyrosine kinase 2 (Pyk2) and integrin alphaVbeta3. Journal of cell science *114*, 2775-2786.
Poincloux, R., Lizarraga, F., and Chavrier, P. (2009). Matrix invasion by tumour cells: a focus on MT1-MMP trafficking to invadopodia. Journal of cell science *122*, 3015-3024.
Sakai, T., Jove, R., Fassler, R., and Mosher, D.F. (2001). Role of the cytoplasmic tyrosines of beta 1A integrins in transformation by v-src. Proc Natl Acad Sci U S A *98*, 3808-3813.
Shattil, S.J., Kim, C., and Ginsberg, M.H. (2010). The final steps of integrin activation: the end game. Nat Rev Mol Cell Biol *11*, 288-300.
Spinardi, L., Rietdorf, J., Nitsch, L., Bono, M., Tacchetti, C., Way, M., and Marchisio, P.C. (2004). A dynamic podosome-like structure of epithelial cells. Exp Cell Res *295*, 360-374.
Steffen, A., Le Dez, G., Poincloux, R., Recchi, C., Nassoy, P., Rottner, K., Galli, T., and Chavrier, P. (2008). MT1-MMP-dependent invasion is regulated by TI-VAMP/VAMP7. Curr Biol *18*, 926-931.
Stroeken, P.J., van Rijthoven, E.A., Boer, E., Geerts, D., and Roos, E. (2000). Cytoplasmic domain mutants of beta1 integrin, expressed in beta 1-knockout lymphoma cells, have distinct effects on adhesion, invasion and metastasis. Oncogene *19*, 1232-1238.
Tarone, G., Cirillo, D., Giancotti, F.G., Comoglio, P.M., and Marchisio, P.C. (1985). Rous sarcoma virus-transformed fibroblasts adhere primarily at discrete protrusions of the ventral membrane called podosomes. Experimental cell research *159*, 141-157.
Tatin, F., Varon, C., Genot, E., and Moreau, V. (2006). A signalling cascade involving PKC, Src and Cdc42 regulates podosome assembly in cultured endothelial cells in response to phorbol ester. Journal of cell science *119*, 769-781.
Uekita, T., Itoh, Y., Yana, I., Ohno, H., and Seiki, M. (2001). Cytoplasmic tail-dependent internalization of membrane-type 1 matrix metalloproteinase is important for its invasion-promoting activity. The Journal of cell biology *155*, 1345-1356.
Vignjevic, D., and Montagnac, G. (2008). Reorganisation of the dendritic actin network during cancer cell migration and invasion. Semin Cancer Biol *18*, 12-22.
Weaver, A.M. (2006). Invadopodia: specialized cell structures for cancer invasion. Clin Exp Metastasis *23*, 97-105.
Wheeler, A.P., and Ridley, A.J. (2007). RhoB affects macrophage adhesion, integrin expression and migration. Experimental cell research *313*, 3505-3516.

Yoneda, T., Lowe, C., Lee, C.H., Gutierrez, G., Niewolna, M., Williams, P.J., Izbicka, E., Uehara, Y., and Mundy, G.R. (1993). Herbimycin A, a pp60c-src tyrosine kinase inhibitor, inhibits osteoclastic bone resorption in vitro and hypercalcemia in vivo. J Clin Invest *91*, 2791-2795.
Zambonin-Zallone, A., Teti, A., Grano, M., Rubinacci, A., Abbadini, M., Gaboli, M., and Marchisio, P.C. (1989). Immunocytochemical distribution of extracellular matrix receptors in human osteoclasts: a beta 3 integrin is colocalized with vinculin and talin in the podosomes of osteoclastoma giant cells. Exp Cell Res *182*, 645-652.

FIGURE LEGENDS

Figure 1: **Extracellular matrix sensing by β1 and β3 integrins controls invadosome formation and localization.**
A) Most SrcYF-expressing cells formed invadosome rosettes (visualized by F-actin staining, in green) only on the adhesive surface (gelatin-TRITC, in red, mixed with vitronectin) and not on anti-adhesive areas (Pluronic F127™, black areas). B) Invadosome rosettes stained by phalloidin-TRITC show higher affinity for vitronectin-FITC (light gray bands), sensed by members of the β3 integrin family, than for fibronectin (black bands), sensed by members of both the β1 and β3 integrin families. C) β1 and β3 integrins show distinct patterns of localization, observed in MEF-SrcYF cells. β3 (in green in merge) highly colocalized with F-actin while β1 staining is limited to the rosette periphery. D) 9EG7 antibothy β1 staining is specific of the activated form of the integrin. Antibody against activated form of β1 directly conjugated to FITC (9EG7-FITC) was added externally and localized around the invadosome visualized by cortactin-mRFP (in red in merge) expressed in live MEF-SrcYF cells. Bars represent 5 μm (A, B), 4 μm (C), and 2 μm (D).

Figure 2**: β1A, and not β3, integrin is essential for invadosome formation.**
A) β3 is not essential for invadosome formation and self-assembly into rosettes, visualized by F-actin (in red in merge) and phospho-Y397-FAK (in blue in merge) staining, which occurs in both MEF-SrcYF β3 +/+ or -/- cells. B) In contrast, β1 depletion in MEF-SrcYF $\beta1^{LoxP/LoxP}$ expressing the CRE recombinase for 96 h resulted in the disappearance of isolated invadosomes or in rosettes probed by phalloidin staining. C) Quantification of the percentage of cells forming invadosomes reveals that almost 95% of MEF-SrcYF $\beta1^{LoxP/LoxP}$ treated with CRE recombinase did not form this structure 4 d post infection (n = 650 counted cells per condition). D) Quantification by qPCR shows an average decrease of 95% in the level of β1 mRNA 96 h post-CRE treatment. Bars represents 3 μm (A) and 10 μm (B).

Figure 3: **Activation of β1 stimulates invadosome auto-assembly.**
A) β1 depletion in pOBL-SrcYF induced the disappearance of invadosomes, shown by phalloidin staining of F-actin. Bar represents 5 μm. B) β1 depletion does not affect Src activation. Lysates of pOBL-SrcYF $\beta1^{+/+}$ and $^{-/-}$ were probed by Western blotting for phospho-SrcY416, a marker of Src activation, total Src, and actin. C) Amino-acyl sequence of the cytoplasmic domain of β1A integrin and the location of the main mutation that activates this integrin. D) Expression of the preactivated mutants of β1 (β1 D759A) in pOBL-SrcYF $\beta1^{-/-}$ cells dramatically increases the number of invadosome rosettes per air unit, while β1WT mutant rescue the rosette number up to the control level.

Figure 4: **PKC regulates invadosome auto-assembly by phosphorylating S785 of β1A integrins.**
A) PKC activation by a 60-min treatment of pOBL-SrcYF cells with 2 μM PMA induces a massive increase in invadosome rosette autoassembly, visualized by phalloidin staining. B) Extracted images from time series (in minutes) from representative observations of pOBL-SrcYF cells expressing GFP-actin and treated with either DMSO (control), the PKC activator PMA (2 μM), and the PKC inhibitor Bim (5 mM). PKC activity regulates the dynamics and maintenance of the invadosome autoassembly state. C) Amino-acyl sequence of the cytoplasmic domain of β1A integrin and the location of the main PKC targets. D) Quantification of invadosomes per Airy unit (AU) shows that a mutation mimicking a constitutive phosphorylated form of Ser 785 (Asp or Glu) dramatically increases the formation of rosettes in pOBL-SrcYF $\beta1^{-/-}$ cells. The non-phosphorylatable mutant of β1 at this site (S785A) has no effect on rosette formation. E) The number of rosettes/AU was quantified in pOBL-SrcYF cells treated with 2 μM PMA or simultaneously with PMA and 5 mM BIM for 60 min. The inhibitory effect of BIM was determined by calculating the percent inhibition of invadosome rosette formation. Mutants mimicking a constitutively phosphorylated Ser785 (S785D and S785E) show only 50% inhibition after BIM treatment, indicating that this residue on β1 is a major target of PKC in the regulation of invadosome autoassembly. Bars represent 20 μm (A) and 5 μm (B).

Figure 5: **β1 activity and signaling control invadosome ECM degradation activity.**
A) Quantification of the degraded surface of gelatin-Oregon Green per cell reveals that β1 has an essential function in this invadosome function. Surprisingly, expression of the activated mutant of β1 (D759A) induces numerous invadosome rosettes associated with poor degradation activity. Moreover, constitutive activation of the signaling pathway downstream of phosphorylation of Ser 785 strongly stimulates ECM degradation. B) β1 also controls the quality of the degradation, as revealed by quantification of the average intensity of the resorbed areas. The few areas degraded in the pOBL-SrcYF $\beta1^{-/-}$ cells are poorly digested since they are close to the maximal fluorescence intensity of a non-digested surface (255) in comparison to pOBL-SrcYF $\beta1^{+/+}$ cells (values closer to 0 indicate a totally black, completely digested area). Between 600 and 1050 cells were counted per condition. C) Representative images extracted from the time series of pOBL-SrcYF $\beta1^{-/-}$ cells expressing or not expressing either human β1 WT, D759A, S785A, or S785D spread on a layer of degradable gelatin-Oregon green. Bar represents 10 μm.

Figure 6: **Photo-inactivation revealed role of β1 in maintaining invadosome self-assembly.**
A) Representative images extracted from time series of MEF-SrcYF $\beta1^{-/-}$ cells expressing human β1-KillerRed™ and GFP-actin. Exogenous human β1-KillerRed™ is functional in rescuing invadosome formation and its proper localization at the periphery. Exposure of KillerRed™ to light for 45 s is followed by fluctuations in intensity and disorganization of GFP-actin in the invadosome rosette. B) Representative images extracted from time series of MEF-SrcYF $\beta1^{-/-}$ cells expressing human β1-pTagRFP™, which has the same excitation/emission spectrum but is much more photostable than KillerRed, and GFP-actin. Light irradiation without ROS production is not sufficient to dissociate invadosomes. C) Representative images extracted from time series of MEF-SrcYF $\beta1^{-/-}$ cells expressing human β1-KillerRed™ and human β1-GFP. These two proteins colocalized, but ROS production at this level of β1-KillerRed™ has no effect on either β1-GFP stability or on any other important proteins for invadosome integrity because invadosomes are still present when β1-KillerRed™

is photo-inactivated. Moreover, β1-KillerRed™ depletion did not affect β1-GFP behaviour in comparison to β1-GFP present in untreated invadosome visualized by cortactin-pTRFP.
D) Photo-inactivation of β1-KillerRed leads to rapid and specific disorganization of invadosomes. Histograms, show the distribution of the percentage of cells where invadosomes are disorganized at various times after light irradiation. X-axis shows time in minutes. Twelve to thirty-nine cells per condition were monitored. Bars represents 3 μm (A,B,C).

Figure 7: **β1 photo-inactivation leads to the loss of cortactin, disorganization of adhesion molecules within the invadosome metastructures, and induction of large, β3-rich focal adhesions.**
A) Representative images extracted from time series of MEF-SrcYF $\beta1^{-/-}$ cells expressing human β1-KillerRed™ and GFP-cortactin. Photo-inactivation of β1-KillerRed™ is followed by a slow decrease in GFP-cortactin fluorescence and its complete disappearance. B) Representative images extracted from time series of MEF-SrcYF $\beta1^{-/-}$ cells expressing both human β1-KillerRed™ and GFP-paxillin. β1 photo-inactivation leads to GFP-paxillin disorganization and decrease in intensity but, in contrast to what is observed with GFP-cortactin, GFP-paxillin remains associated with the invadosome. C) Representative images extracted from time series of MEF-SrcYF $\beta1^{-/-}$ cells expressing human β1-KillerRed™ and β3-GFP. β1 photo-inactivation leads to slow dissociation of invadosomes and the massive formation of β3-rich focal adhesions (red arrows). Bars represents 3 μm (A, B, C).

SUPPLEMENTARY INFORMATION

SUPPLEMENTARY FIGURE LEGEND

Figure S1: A MEF-YFSrc adhesion on micropatterned stripes of FITC-vitronectin (green fluorescence) and fibronectin (unlabeled). Actin is stained by TRITC-phalloïdin. The invadosome rosette is localized at the interface between vitronectin and fibronectin. Bar is 10 μm. B MEF-YFSrc adhesion on micro-patterned stripes of FITC-vitronectin (green fluorescence) width 10 μm, and either unlabeled laminins (right panel) or laminins (left panel (unlabeled). Actin is stained by TRITC-phalloïdin. C Quantification of the localization of invadosome rosettes on double patterned substrates.

Figure S2: The number of rosettes/AU was quantified in pOBL-SrcYF cells treated with 2 μM PMA or simultaneously with PMA and 5 mM BIM for 60 min. The inhibitory effect of BIM was determined by calculating the percent inhibition of invadosome rosette formation. Mutants mimicking a constitutively phosphorylated Ser785 (S785D and S785E) show only 50% inhibition after BIM treatment, indicating that this residue on β1 is a major target of PKC in the regulation of invadosome autoassembly.

SUPPLEMENTARY MOVIE LEGENDS

Supplementary Movie 1: Live imaging (0,05Hz) of invadosome rosette visualized by GFP-actin (TIRF microscopy) and β1-KillerRed™ (epifluorescence microscopy), followed by 50 s of red light irradiation to photo-inactivate β1-KillerRed™.

Supplementary Movie 2: Live imaging (0,05Hz) of invadosome rosette visualized by GFP-actin (TIRF microscopy) and β1-TagRFP™ (epifluorescence microscopy), followed by 45 s of red light irradiation, which does not photo-inactivate, but just bleaches, β1-TagRFP™.

Supplementary Movie 3: Live imaging (0,025Hz) of invadosome rosette visualized by peripheral signals of β1-GFP (TIRF microscopy) and β1-KillerRed™ (epifluorescence microscopy), followed by 45 s of red light irradiation to photo-inactivate β1-KillerRed™.

Supplementary Movie 4: Live imaging (0,05Hz) of invadosome rosette visualized by cortactin-GFP (TIRF microscopy) and β1-KillerRed™ (epifluorescence microscopy), followed by 50 s of red light irradiation to photo-inactivate β1-KillerRed™.

Supplementary Movie 5: Live imaging (0,05Hz) of invadosome rosette visualized by paxillin-GFP (TIRF microscopy) and β1-KillerRed™ (epifluorescence microscopy), followed by 45 s of red light irradiation to photo-inactivate β1-KillerRed™.

Supplementary Movie 6: Live imaging (0,016Hz) of invadosome rosette visualized by β3-GFP (TIRF microscopy) and β1-KillerRed™ (epifluorescence microscopy), followed by 45 s of red light irradiation to photo-inactivate β1-KillerRed™.

Supplementary Movie 7: Live imaging (0,1Hz) of invadosome rosette visualized by GFP-actin (TIRF microscopy) and β1-KillerRed™ (epifluorescence microscopy), followed by 45 s of red light irradiation to photo-inactivate β1-KillerRed™.

Supplementary Movie 8: Live imaging (0,0083Hz) of invadosome rosette visualized by β1-GFP (TIRF microscopy) and cortactin-pTRFP (epifluorescence microscopy) under normal conditions.

Figure 1:

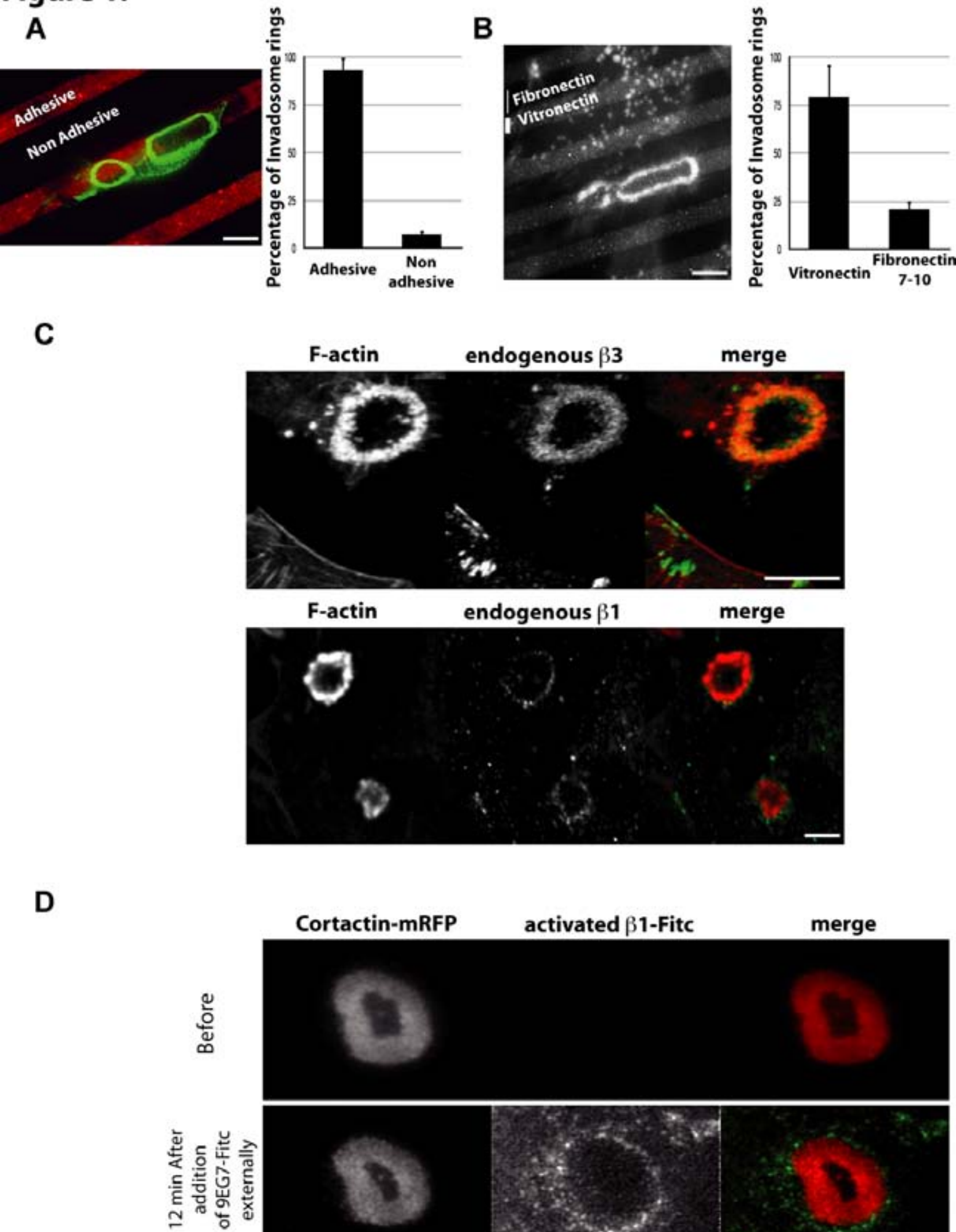
A
Adhesive
Non Adhesive
Percentage of Invadosome rings
100
75
50
25
0
Adhesive
Non adhesive
B
Fibronectin
Vitronectin
Percentage of Invadosome rings
100
75
50
25
0
Vitronectin
Fibronectin 7-10
C
F-actin
endogenous β3
merge
F-actin
endogenous β1
merge
D
Cortactin-mRFP
activated β1-Fitc
merge
Before
12 min After addition of 9EG7-Fitc externally

Figure 2:

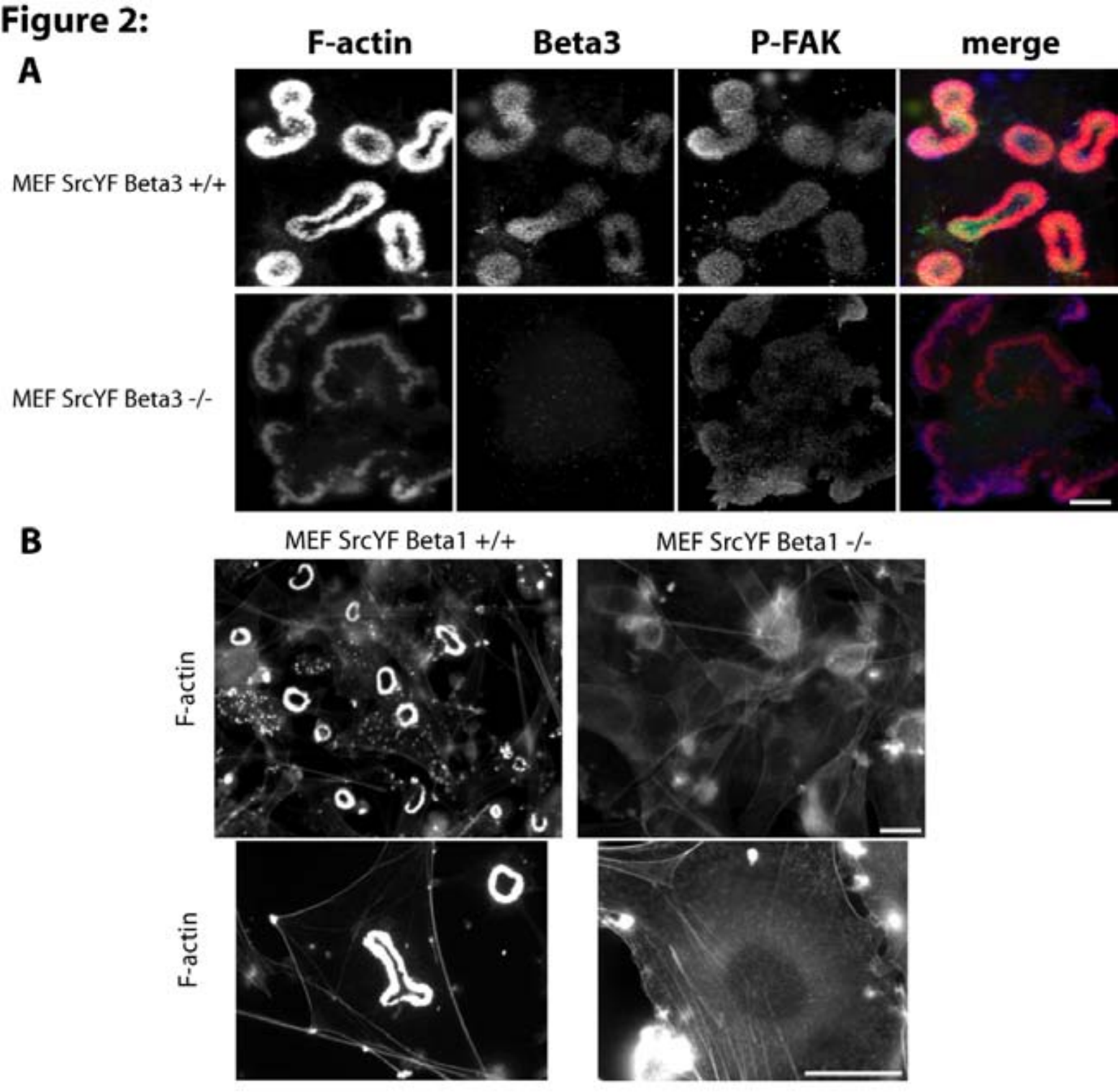
A
F-actin
Beta3
P-FAK
merge
MEF SrcYF Beta3 +/+
MEF SrcYF Beta3 -/-
B
MEF SrcYF Beta1 +/+
MEF SrcYF Beta1 -/-
F-actin
F-actin

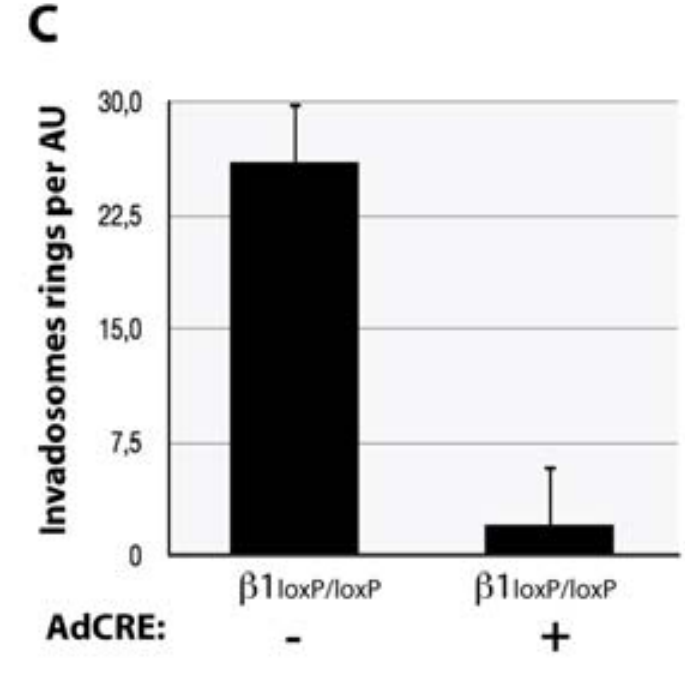
C
Invadosomes rings per AU
30,0
22,5
15,0
7,5
0
β1loxP/loxP
β1loxP/loxP
AdCRE:
-
+

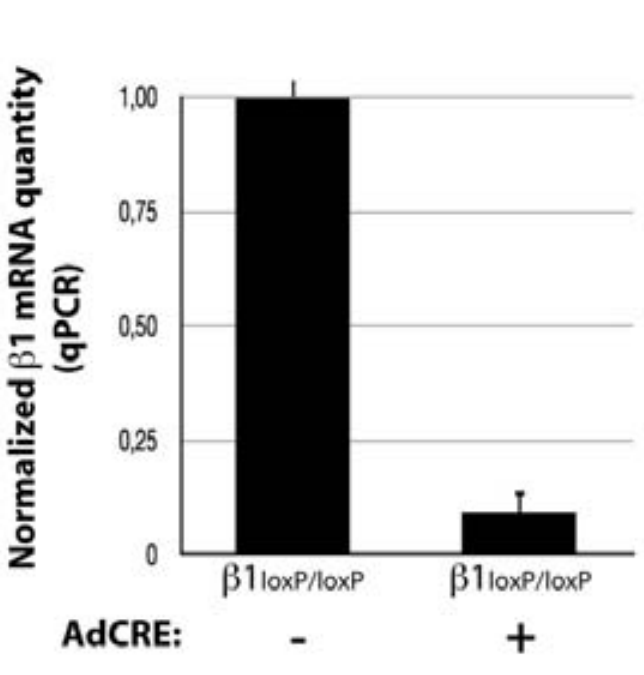
D
Normalized β1 mRNA quantity (qPCR)
1,00
0,75
0,50
0,25
0
β1loxP/loxP
β1loxP/loxP
AdCRE:
-
+

Figure 3:

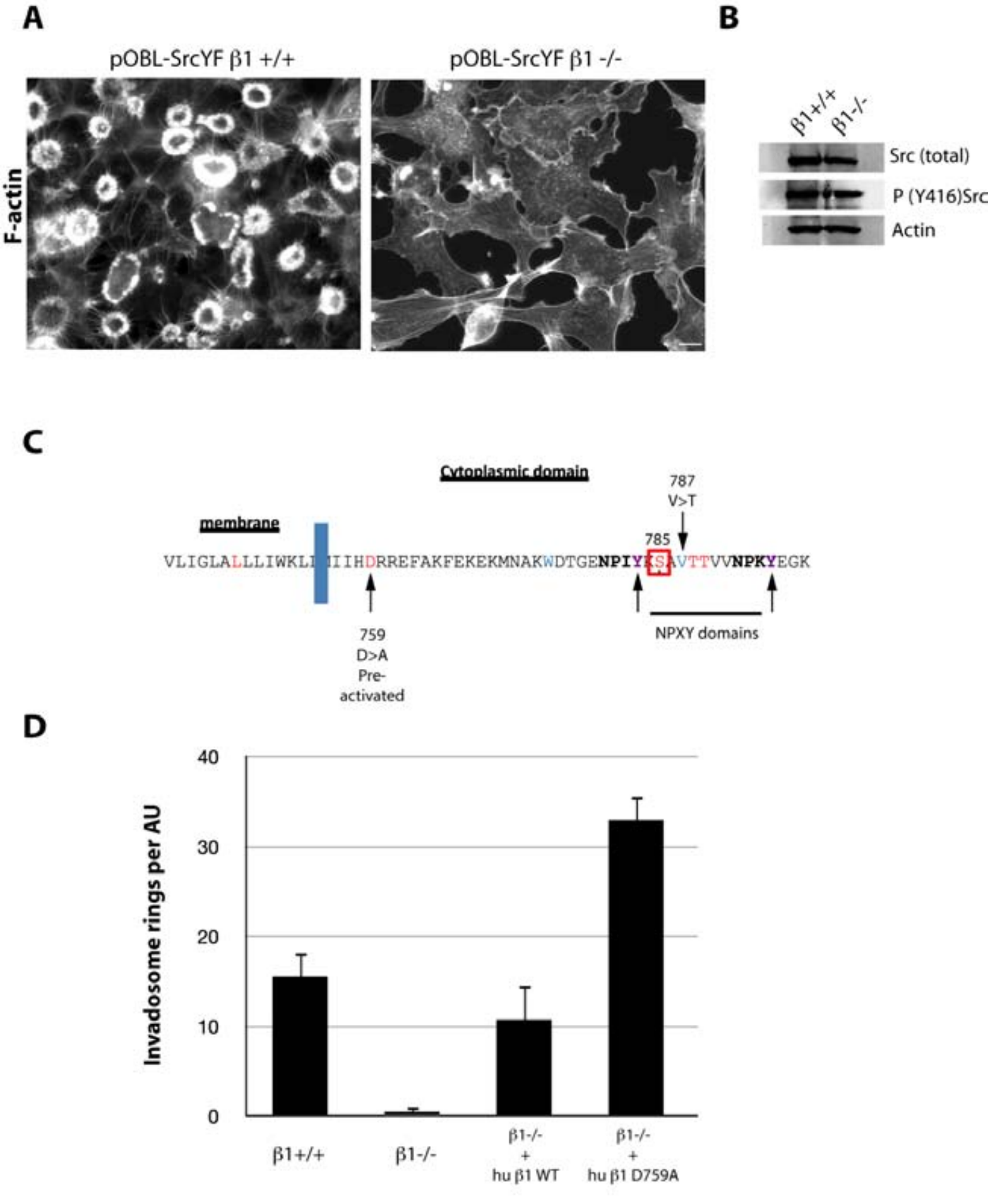
A
pOBL-SrcYF β1 +/+
pOBL-SrcYF β1 -/-
F-actin
B
β1+/+
β1-/-
Src (total)
P (Y416)Src
Actin
C
Cytoplasmic domain
787
V>T
membrane
785
VLIGLALLLIWKLIIIHDRREFAKFEKEKMNAKWDTGENPIYKSAVTTVVNPKYEGK
759
D>A
Pre-
activated
NPXY domains
D
Invadosome rings per AU
40
30
20
10
0
β1+/+
β1-/-
β1-/-
+
hu β1 WT
β1-/-
+
hu β1 D759A

Figure 4:

A

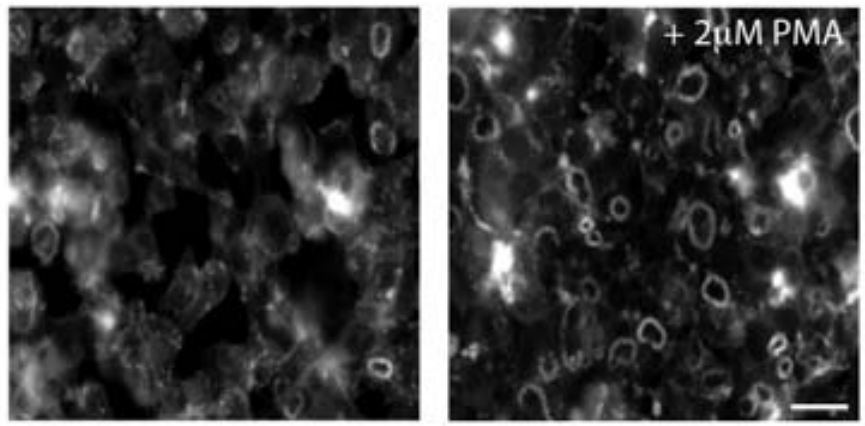

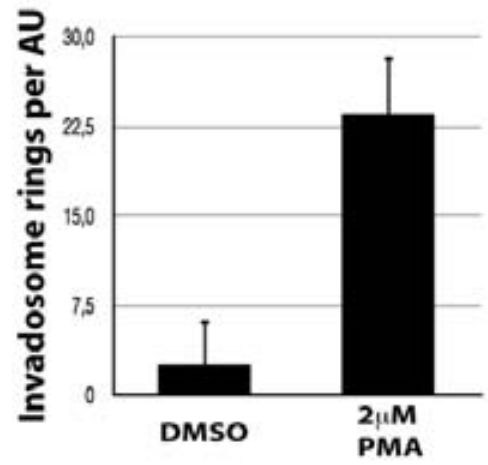

B

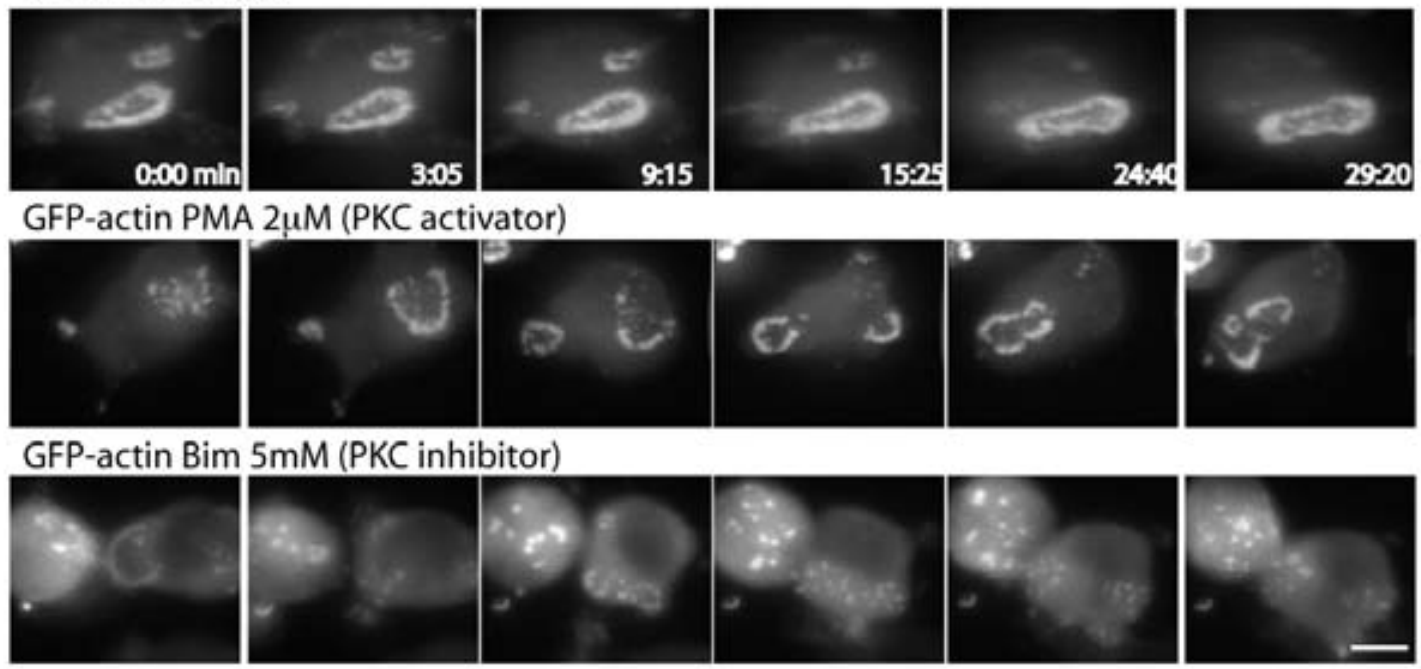

C

D

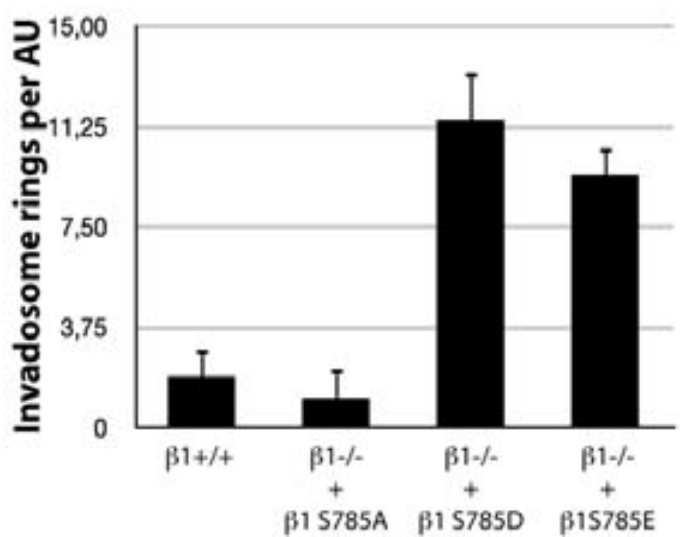

E

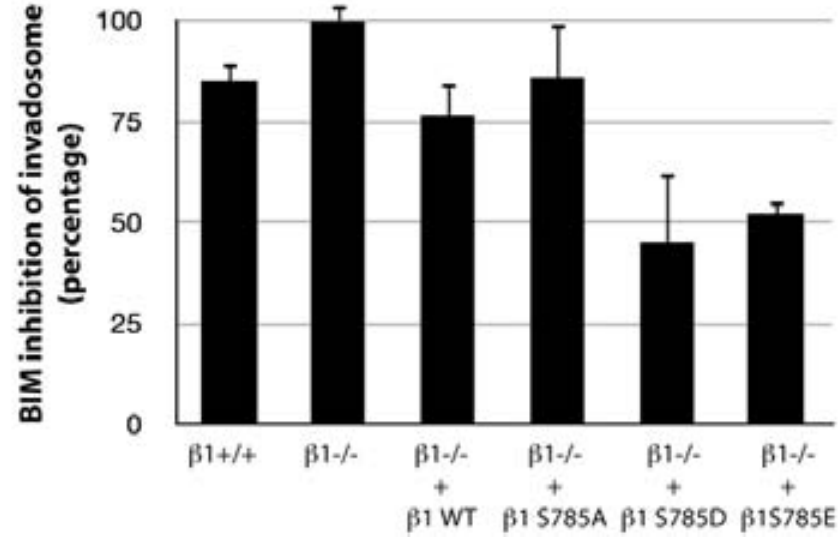

Figure 5:

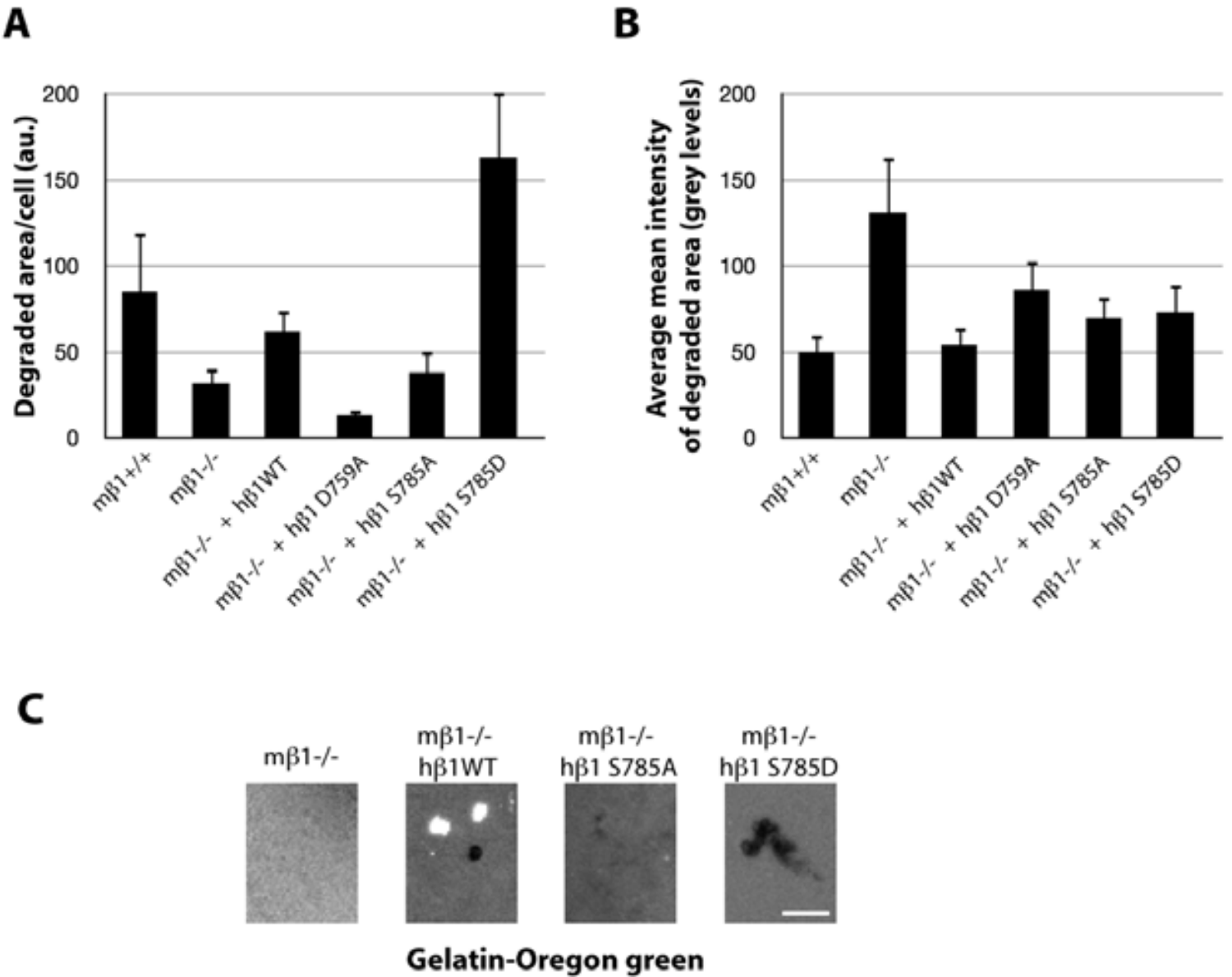
A
Degraded area/cell (au.)
200
150
100
50
0
mβ1+/+
mβ1-/-
mβ1-/- + hβ1WT
mβ1-/- + hβ1 D759A
mβ1-/- + hβ1 S785A
mβ1-/- + hβ1 S785D
B
Average mean intensity of degraded area (grey levels)
200
150
100
50
0
mβ1+/+
mβ1-/-
mβ1-/- + hβ1WT
mβ1-/- + hβ1 D759A
mβ1-/- + hβ1 S785A
mβ1-/- + hβ1 S785D
C
mβ1-/-
mβ1-/- hβ1WT
mβ1-/- hβ1 S785A
mβ1-/- hβ1 S785D
Gelatin-Oregon green

Figure 6:

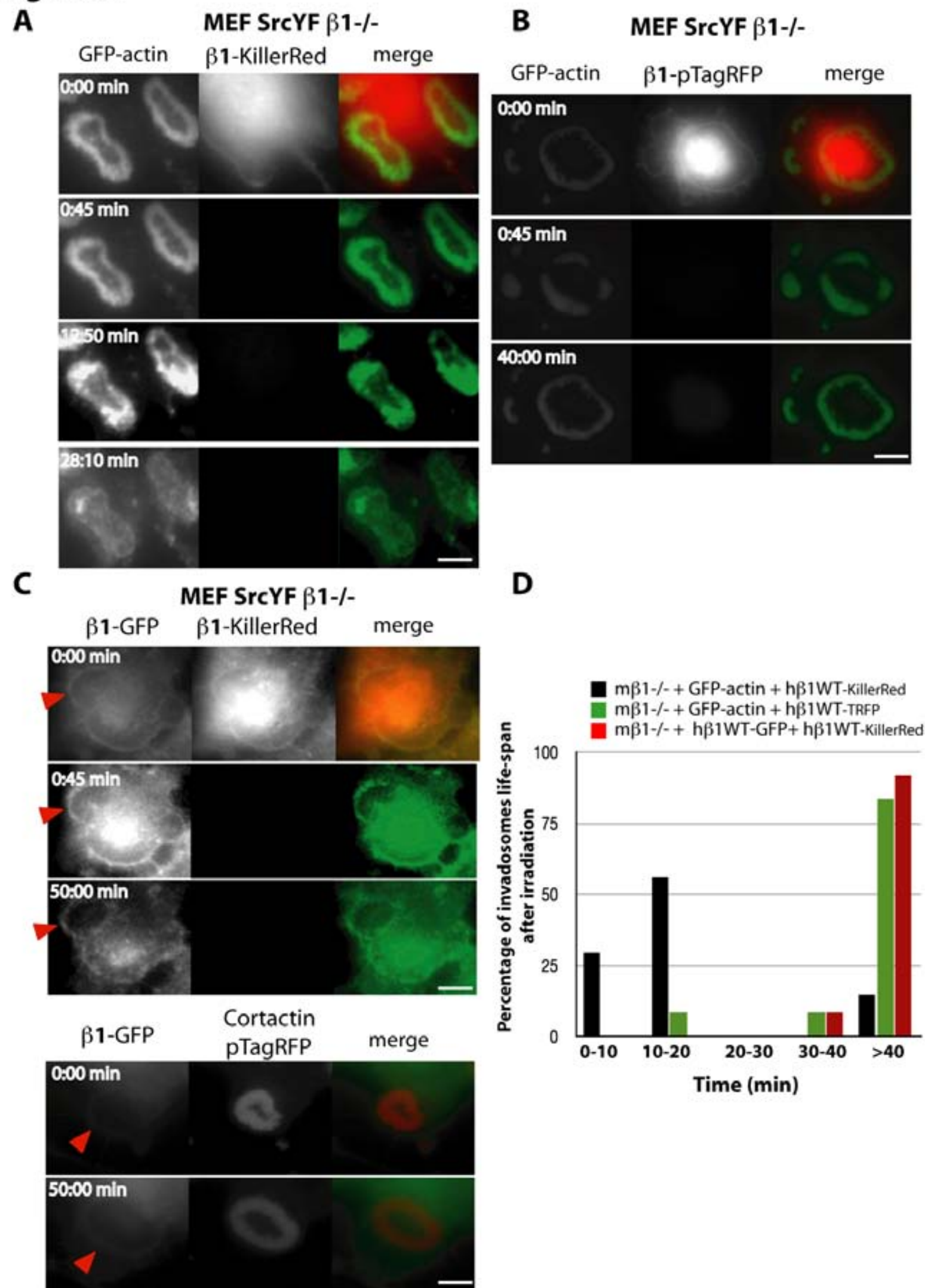
A
MEF SrcYF β1-/-
GFP-actin
β1-KillerRed
merge
0:00 min
0:45 min
28:10 min
B
MEF SrcYF β1-/-
GFP-actin
β1-pTagRFP
merge
0:00 min
0:45 min
40:00 min
C
MEF SrcYF β1-/-
β1-GFP
β1-KillerRed
merge
0:00 min
0:45 min
50:00 min
β1-GFP
Cortactin pTagRFP
merge
0:00 min
50:00 min
D
mβ1-/- + GFP-actin + hβ1WT-KillerRed
mβ1-/- + GFP-actin + hβ1WT-TRFP
mβ1-/- + hβ1WT-GFP+ hβ1WT-KillerRed
Percentage of invadosomes life-span after irradiation
100
75
50
25
0
0-10
10-20
20-30
30-40
>40
Time (min)

Figure 7:

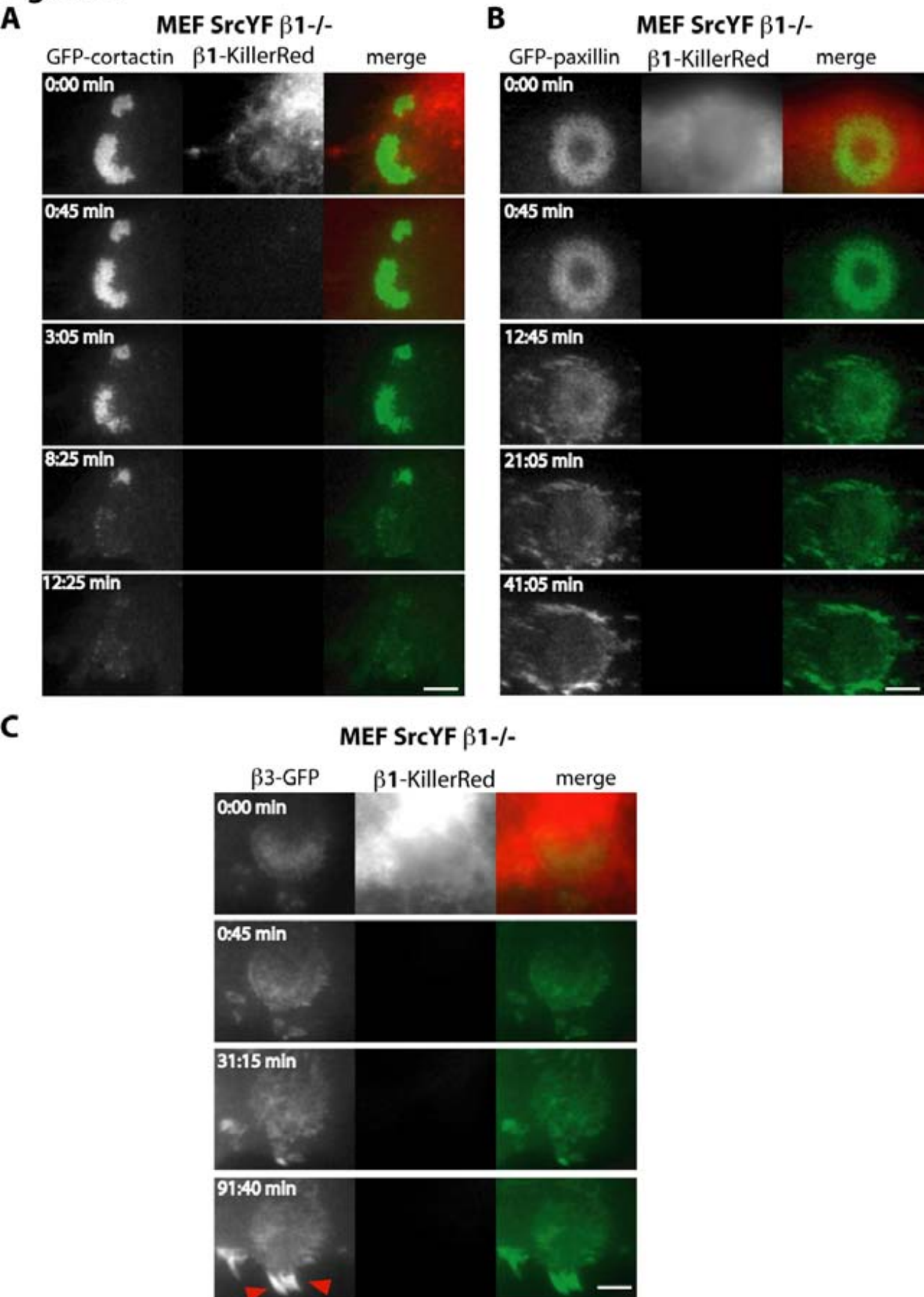
A
MEF SrcYF β1-/-
GFP-cortactin
β1-KillerRed
merge
0:00 min
0:45 min
3:05 min
8:25 min
12:25 min
B
MEF SrcYF β1-/-
GFP-paxillin
β1-KillerRed
merge
0:00 min
0:45 min
12:45 min
21:05 min
41:05 min
C
MEF SrcYF β1-/-
β3-GFP
β1-KillerRed
merge
0:00 min
0:45 min
31:15 min
91:40 min

A

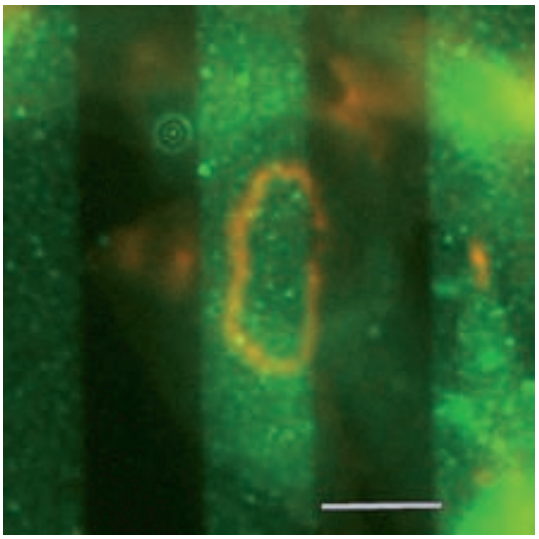

B

Collagen/Vitronectin

Laminin/Vitronectin

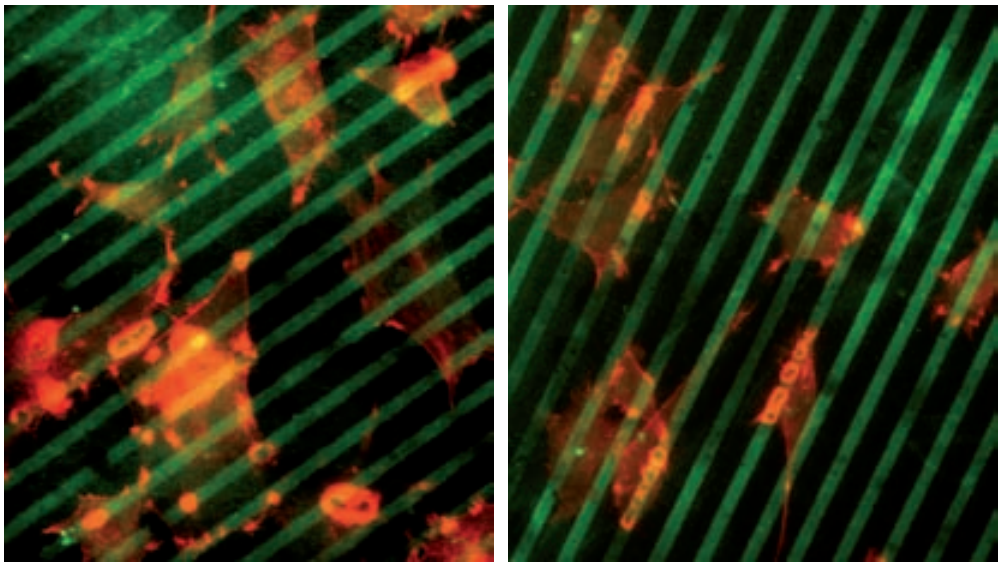

C

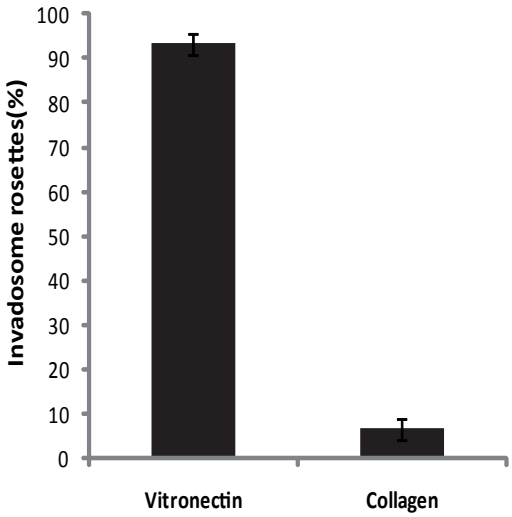

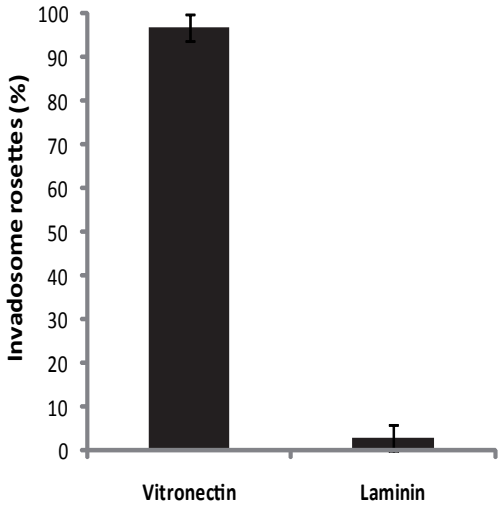

Figure S1

Figure S2:

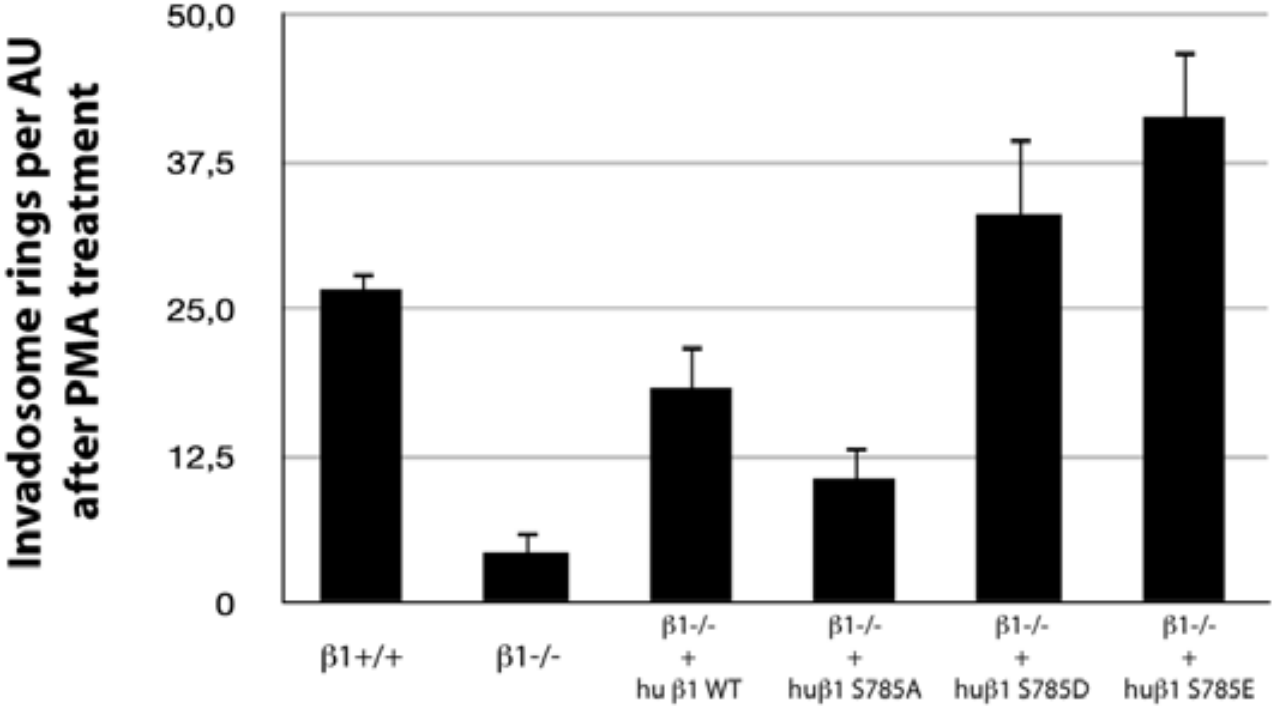
Invadosome rings per AU after PMA treatment
50,0
37,5
25,0
12,5
0
β1+/+
β1-/-
β1-/- + hu β1 WT
β1-/- + huβ1 S785A
β1-/- + huβ1 S785D
β1-/- + huβ1 S785E